ABSTRACT

HIGH-SPIN STRUCTURE OF ^{116}Sb AND ^{118}Sb

By

Wayne Harold Bentley

The high-spin structure of ^{116,118}Sb has been studied using the techniques of in-beam gamma-ray spectroscopy. Experiments performed include gamma-ray angular distributions, γ-γ-t coincidence measurements, gamma-ray excitation functions, and gamma-ray half-life measurements. The reactions used to populate the high-spin levels were proton, alpha, and lithium induced fusion evaporation reactions. Level schemes for each of these nuclei have been constructed from the results of these experiments.

The level schemes display behavior that can be explained only by assuming the existance of both deformed and spherical states. Such coexistance of states has previously been observed in neighboring nuclei. This investigation extends these findings to the odd-odd Sb nuclei. A qualitative discussion of these various structures is made in terms of the shell model and the particle-plus-deformed-rotor model.

HIGH-SPIN STRUCTURE OF ^{116}Sb AND ^{118}Sb

By

Wayne Harold Bentley

A DISSERTATION

Submitted to

Michigan State University

in partial fulfillment of the requirements

for the degree of

DOCTOR OF PHILOSOPHY

Department of Physics

1980

ACKNOWLEDGEMENTS

I wish to thank Dr. W. H. Kelly for his encouragement and assistance during the experimental work and for his never-ending patience during the preparation of this thesis.

I would also like to thank Dr. R. A. Warner, Dr. C. B. Morgan, Dr. S. R. Faber, Dr. R. B. Firestone, Mr. K. Shafer, Mr. J. A. Carr and Mr. M. F. Slaughter for their help during experiments and for teaching me much of what I have learned.

I wish to thank Dr. F. Venezia, Dr. J. W. Mihelich and Dr. E. G. Funk for assistance with those experiments performed using the accelerator facilities of Notre Dame.

I wish to thank Dr. P. M. Walker, Dr. R. M. Ronningen and Dr. W. C. McHarris for many valuable discussions concerning the interpretation of the results, as well as their suggestions during the preparation of this thesis.

Special thanks go to Dr. P. S. Miller, Dr. H. Laumer and D. W.-S. Chien for their assistance in setting up and running the M.S.U. cyclotron. Thanks also go to the remainder of the cyclotron staff for their never-ending assistance during all phases of this project.

Finally, I wish to thank Mrs. T. Awes for typing this manuscript and the N.S.F. for financial support.

TABLE OF CONTENTS

LIST OF TABLES

LIST OF FIGURES

I. INTRODUCTION

Until recently, nuclear structure physics, both experimental and theoretical, has concentrated primarily on even-even and odd-mass nuclei. This is mainly because of the complexities involved in studying odd-odd nuclei. However, with increased understanding of odd-mass nuclei and improvements in experimental techniques, much greater attention is now being given to understanding odd-odd nuclei. Continuing in this direction, the present study of the high spin structure of the two odd-odd nuclei ^{116,118}Sb was undertaken. The goal of this work was experimentally to determine high-spin level structures and attempt to gain an understanding of these results in terms of existing theories.

There are many reasons for studying odd-odd nuclei, the most fundamental of which is to obtain information on the residual proton-neutron interaction. An understanding of this interaction is a necessary part in forming a complete description of nuclear structure. Such an understanding can come only after the level scheme systematics from a large number of odd-odd nuclei distributed over the entire mass range has been collected. The results obtained in this study will contribute to that collection of data. In addition, recent interest has developed in high-spin rotational structure in odd-odd transitional nuclei. Since in odd-odd nuclei there are two unpaired particles that can occupy high-spin single-particle levels, it is possible to form high-spin states at relatively low excitation energy.

Such states are presently being studied theoretically (cf. ref. 1). However, very little experimental information is available to compare with this work. Since low-lying deformed states were previously known to exist in the odd-mass Sb nuclei,[2] it was reasonable to expect similar low-lying deformed states to exist in the neighboring odd-odd nuclei. Such considerations indicated that interesting phenomena should exist in the high-spin level structure of ^{116,118}Sb.

Much previous work has been done studying Sb nuclei both at Michigan State University and elsewhere. The low-spin states of ^{116,117,118,119}Sb have been studied using the (p,nγ) reaction.[3-6] In addition, the high-spin states of ^{113,115,117,119}Sb have been studied using the (^{6}Li,3nγ) reaction.[7] The results of these studies proved to be invaluable in sorting out and identifying the gamma-rays belonging to ^{116,118}Sb. In fact, in general a study of an odd-odd nucleus would prove to be nearly impossible without first having a partial knowledge of the structure of neighboring nuclei.

In addition to these experimental studies, theoretical attempts have also been made at describing Sb nuclei. Except in the case of ^{118}Sb, various model calculations[8,9] have been carried out and compared with all of the previously mentioned experimental results. In particular, much effort has been expended in attempting to quantitatively describe the rotational bands in the odd-mass Sb nuclei.[10-13]

The next chapter of this thesis is a brief discussion of some of the theoretical models used in describing nuclear structure. Chapter III includes a general discussion of the types of experiments performed in this study. In chapters IV and V the experimental results are presented for ^{116}Sb and ^{118}Sb, respectively, including a discussion of the construction of the respective level schemes. The final chapter contains a qualitative comparison of these results to the models.

II. THEORETICAL CONSIDERATIONS

A. Nuclear Shell Model

The nuclear shell model was developed in 1949 independently by M. G. Mayer[14] and Haxel, Jensen, and Suess.[15] The assumptions behind this model are very similar to those upon which the atomic shell model is based. Each particle is assumed to move in an independent orbit. Therefore the interaction between each particle and all of the other particles can be replaced with an interaction involving the particle and some average potential. In order to reproduce the experimentally determined ordering of the shell model states, a large spin-orbit coupling term was required as part of this potential. One of the effects of this spin-orbit term is the lowering of selected states into the next lower major shell. These lowered states then have opposite parity and higher spin values than the remaining states in the shell. These states are referred to as unique-parity states. Examples of states of this type include the $1g_{9/2}$, $1h_{11/2}$ and $1i_{13/2}$ orbitals.

In real nuclei, however, the nucleons do not move in completely independent orbits. There is a residual interaction between particles in each subshell. This interaction is observable in the last subshell, if it is not completely filled. A large part of the residual interaction is the pairing energy which arises between two particles in the same subshell with opposite m_j-values. This is the result of a large overlap in the wave functions of these particles.

Of particular interest in odd-odd nuclei is the residual interaction between the odd proton and the odd neutron. When the odd proton and odd neutron are placed in given single particle orbitals, a multiplet of states results from the various ways of coupling the angular momenta of the two particles. The p-n residual interaction is responsible for the removal of the energy degeneracy of this multiplet. Identification of the various members of these multiplets in odd-odd nuclei gives direct information on the strength and form of this interaction.

Shell model calculations for ^{112,114,116}Sb have been performed by VanGunsteren et. al.[8] In these calculations because Sb has only one proton above the Z=50 closed shell the proton could be treated as a particle. However, in order to include the pairing effects of the several valence neutrons the odd neutron was treated as a quasiparticle. These results were relatively successful in describing the existing low-spin data. There were, however, no high-spin results reported from these calculations.

B. Vibrational Core Excitations

In addition to the single-particle states described by the spherical shell model, other modes of excitations are available. These include collective vibrations of the core. Theoretical treatments of the odd mass Sb nuclei involve single-particle shell model orbitals as well as single-particle states coupled to these phonon excitations of the core.[9] Similarly a complete theoretical description of the

odd-odd Sb nuclei would have to include the possibility of vibrational coupling to the various two-particle shell model states.

C. Deformed States

The Sb nuclei are only one proton away from the Z=50 closed shell. Because of this it would be reasonable to expect that a spherical description of these nuclei should be adequate. However, experiments have shown[7] the singly odd Sb nuclei exhibit evidence for coexistance of deformed states with the spherical states. Band structure properties in the odd mass nuclei have suggested[2] rotational bands built on a permanently deformed, prolate, proton hole state. This interpretation is consistent with calculations of the total potential energy surface,[12] which show a well defined minimum in the energy of the $9^+/2$ {404} proton orbital at a positive deformation value. ($\varepsilon \simeq 0.15$ for ^{117}Sb)

An alternative description based on a vibrational model[13] has also been employed in describing the observed odd mass bands. However, the low-lying $9^+/2$ bandheads are difficult to explain in such a model. Consequently, this likelihood of deformed states in the odd mass Sb nuclei, leaves the odd-odd Sb nuclei as interesting sources of further information.

D. Rotational Model

The foundation for the nuclear rotational model was developed in 1952 by Bohr and Mottelson. This model is based on the average nuclear potential being non-spherical.

The axes determined by this deformed potential are then allowed to rotate in space. This rotation is slow compared to the motion of the individual nucleons, which collectively produce the deformed potential. The Hamiltonian can then be written as two terms, one of which describes the collective rotation of the core, while the second term describes the intrinsic states. These intrinsic states were described by Nilsson and involve single-particle states in a deformed potential. The resultant Hamiltonian is shown in equation (1) and is referred to as the unified model.[16]

$$H = H_{Rot} + H_{int} = \frac{h^2}{2\Theta} \vec{R}^2 \qquad (1)$$

Here Θ represents the moment of inertia.

In this model the total angular momentum $\vec{I}$ is shared between the particle angular momentum $\vec{j}$ and the core angular momentum $\vec{R}$, as can be seen in the following equation:

$$\vec{I} = \vec{R} + \vec{j} \qquad (2)$$

Quantum mechanics requires that R_3, the component of the rotation vector along the symmetry axis, be zero for an axially symmetric core. Using this fact and writing the Hamiltonian explicitly in terms of the particle and core angular momenta results in the following expression:

$$H = H_{int} + \frac{\hbar^2}{2\Theta} (\vec{j}^2 - j_3^2) + \frac{\hbar^2}{2\Theta} (\vec{I}^2 - I_3^2) - \frac{\hbar^2}{2\Theta} (I_+ j_- + I_- j_+) \qquad (3)$$

In this expression the 3-axis is taken to be in the direction of the deformation symmetry axis and the $I_{\pm}, j_{\pm}$ are scalar operators very similar to the rotational raising and lowering operators. ($I_{\pm} = (I_1 \pm iI_2)$, $j_{\pm} = (j_1 \pm ij_2)$). The first two terms in equation (3) refer to the particle motion. The third term refers to the collective motion. The last term, generally referred to as the Coriolis coupling term, contains the interaction between the particle and rotational motion. In the normal rotational model the first two terms are combined to give the intrinsic energy, and the Coriolis term is assumed to be small. This results in normal rotational bands with energies given by the following equation:

$$H = E_{int} + \frac{\hbar^2}{2\Theta} \{I(I+1) - K^2\} \qquad (4)$$

Here K is the component of the total angular momentum along the symmetry axis and in this limit represents a good quantum number. In well deformed nuclei this result works quite well. Deviations from this result can often be explained by treating the Coriolis term as a perturbation, which results in the mixing of bands with different K values. However, if the effect of the Coriolis term becomes large a different approach is needed.

This can be seen by looking at the explicit form of the intrinsic energy as determined in the Nilsson model.[17]

$$H_{int} = e_j + \kappa\beta \{\frac{3\Omega^2 - j(j+1)}{4j(j+1)}\} = e_j + C\Omega^2 \qquad (5)$$

In this equation Ω is the component of $\vec{j}$ along the symmetry axis (Ω=K for an axially symmetric core) and, κ and β are parameters that go into the Nilsson potential. Explicitly, β is a measure of the quadrupole deformation. The parameter C, which is defined by this equation, depends on κ, β and the particle angular momentum $\vec{j}$.

Substituting equation (5) into (3) and rearranging terms results in the following expression for the total Hamiltonian.

$$H = e_j + \frac{\hbar^2}{2\Theta}(\vec{j}^2 + I^2) + (C - \frac{\hbar^2}{\Theta})\Omega^2 - \frac{\hbar^2}{2\Theta}(I_+j_- + I_-j_+) \qquad (6)$$

For a given situation the first two terms of this Hamiltonian are diagonal and the problem resolves to diagonalizing the last two terms. In well deformed nuclei the moment of inertia Θ is large and consequently the Coriolis term is small. In this case the solutions are eigenstates of Ω^2 and the normal strong coupling limit results.

As the total angular momentum $\vec{I}$ increases the importance of the Coriolis term in the Hamiltonian increases also. At sufficiently large $\vec{I}$ this term becomes much larger than the Ω^2 term and the solutions become eigenstates of the Coriolis term. In this limit Ω and K are no longer good quantum numbers, nor is the strong coupling scheme applicable. It has been shown that this situation corresponds to a rotation

aligned coupling scheme described by Stephens.[18] In this scheme the large Coriolis force decouples the particle from the deformed core and aligns it in the direction of the rotation. Now α, the projection of $\vec{j}$ on the rotation axis, is a good quantum number rather than Ω, the projection on the symmetry axis. The particle now contributes to the angular momentum without affecting the energy spacing of the core rotational states.

In addition to the high angular momentum limit the rotation alignment coupling scheme can be extended to low spin states in some cases. This situation occurs when the coefficient of the Ω^2 term in the Hamiltonian is approximately zero. One of the requirements for this to occur is that the Fermi energy level must be near the low Ω orbitals of the j shell. This corresponds to a particle state in prolate nuclei and a hole state in oblate nuclei. An additional requirement is that the value of the deformation parameter be in the approximate range $|\beta| \approx 0.18 \pm 0.08$. Larger values of β result in strong coupling, while smaller values lead to the weak coupling limit. The final condition is that the spin j of the particle should be large. This usually implies that the particle be in one of the high spin unique-parity orbitals, such as the $1i_{13/2}$ or $1h_{11/2}$. For the two nuclei under study here, the Fermi energy for the neutron states is very near the low Ω components of the $1h_{11/2}$ orbital.

E. Extension of the Unified Model

A generalization of this model to include triaxially deformed nuclei has been carried out by Meyer-ter-Vehn.[19] In addition Toki and Faessler[20] have included a variable moment of inertia for the core, which accounts for centrifugal stretching with increased angular momentum. This resulting model has been quite successful in describing a large amount of data on the odd mass transitional nuclei.

In addition work is currently being done by Toki and Faessler to extend this particle-plus-gamma-deformed-rotor model to odd-odd nuclei.[1] In this case two particles must be coupled to the core. They can both couple in the same manner resulting in what Faessler has termed the "peaceful case". Alternatively one of the particles can strongly couple, while the second particle is rotationally aligned, resulting in the "conflicting case."

The Hamiltonian for this model is given as the following:

$$H = H_{Rot} + H_{Shell} + H_{Def} + H_{Pair} + H_{Res}$$

The first term represents the rotational motion of the triaxially deformed core. The next two terms express the single-particle energies of the two particles and their coupling to the deformed core. The final two terms describe the residual pairing interaction between the valance particles and the residual proton-neutron interaction of the

two odd particles. Calculations[20,21] using this model have been carried out for ^{198}Tl and ^{194}Au. The results of these calculations were quite successful in describing these nuclei.

For completeness it should be noted that a similar situation occurs for two quasi-particle states in doubly even nuclei. Experimentally there is presently much interest in the Coriolis effects on two quasi-particle sidebands in these nuclei (cf. ref. 22). Theoretically treatments very similar to those described above have been applied, especially with regards to the effect of the Coriolis interaction in producing backbending. (cf. ref. 23)

The doubly odd Sb nuclei are good candidates for a consideration by this extended rotational model. The neighboring nuclei, both odd-proton Sb and odd-neutron Te nuclei, have demonstrated evidence for the coexistance of deformed states. It is reasonable to expect that the doubly odd Sb nuclei should exhibit similar behavior. In addition the deformation parameter as determined in the odd mass Sb nuclei is sufficiently small so as to allow for the possibility of rotational alignment. This coupled with the knowledge that the neutron Fermi level is located very near the low-Ω substates of the high angular momentum, unique-parity $1h_{11/2}$ orbital, makes rotationally aligned neutron states a very likely possibility. These observations will be considered in detail in the final chapter.

III. EXPERIMENTAL CONSIDERATIONS

A. Fusion Evaporation Reaction

The study of high spin states first requires getting the nucleus of interest into a high energy, high angular momentum excited state. This can be done with a fusion-evaporation reaction. An accelerated beam of heavy-ions, alpha particles, or protons collides with a target of the appropriate enriched isotope. The projectile and target nuclei combine into a highly excited compound system which loses most of its energy through the statistical evaporation of energetic neutrons. Eventually a point is reached where there is no longer sufficient energy to evaporate another neutron. The resulting nucleus is still in a high energy, high angular momentum state that now decays by emitting gamma-rays.

The cross-section as a function of beam energy for producing a given final nucleus is a peak about 10 MeV wide, separated from neighboring peaks by about 15 MeV. An example, showing cross sections for an (α,xn) reaction, calculated using a standard compound nuclear reaction code,[24] is shown in Figure III-1. Small cross-sections for competing reactions which were not calculated include proton and alpha evaporation, as well as direct reactions.

After the compound nucleus has cooled to where it is stable against further particle evaporation, it is still at a very high excitation (about 10 MeV). The density of available states is extremely high at this energy. Because

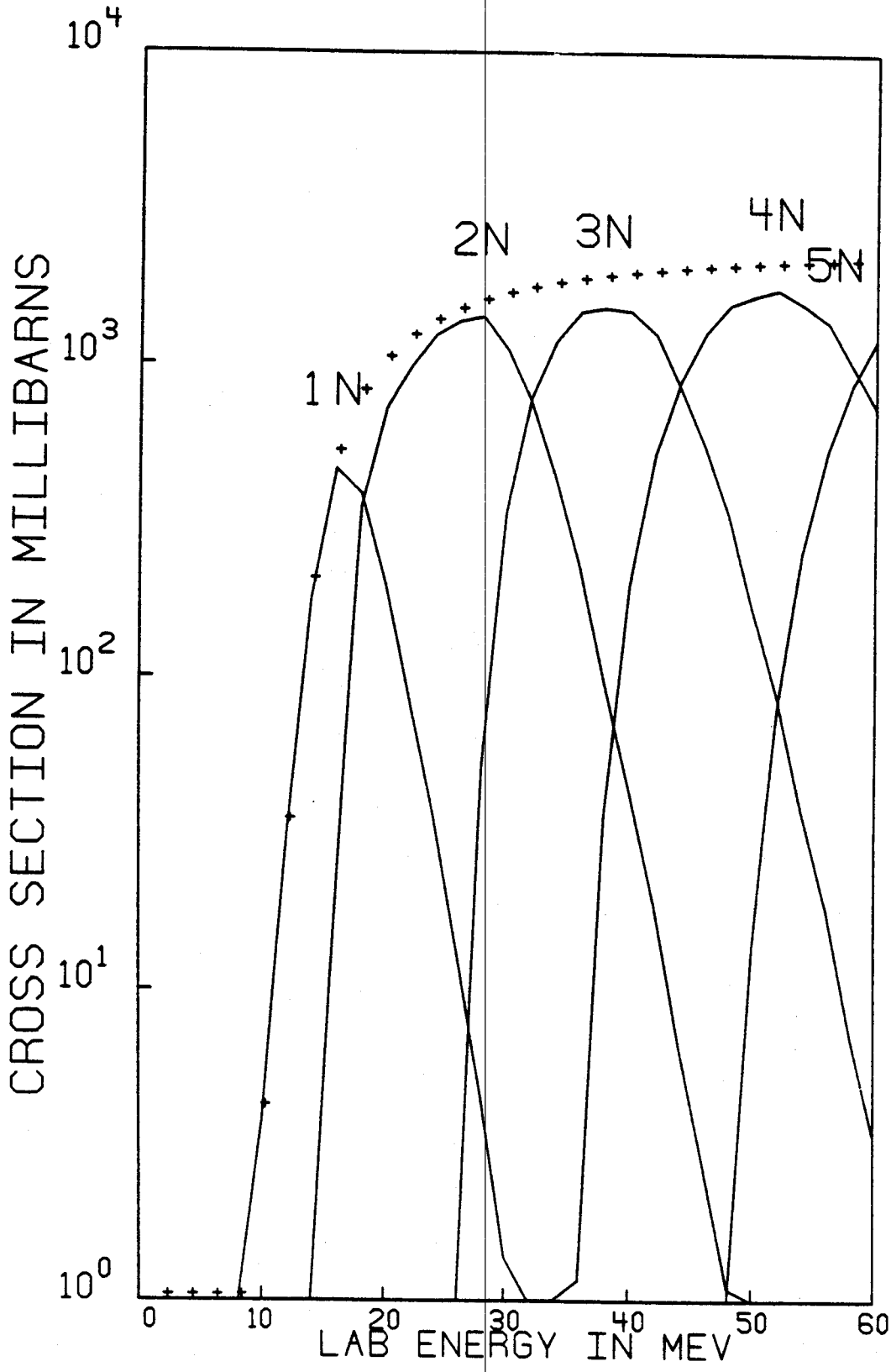

Figure III-1 Cross sections for neutron evaporation as a function of beam energy following an α induced compound nuclear reaction

of the large number of states and the resulting myriad of decay paths, only a statistical continuum of gamma-rays can be detected from this portion of the decay process. This continues until the nucleus has decayed down to the yrast sequence, where yrast is defined as the lowest lying level of a given spin value.[25] At this point the decay proceeds along or near the yrast line down to the ground state. The limited number of available paths during this portion of the decay results in discrete gamma-ray lines appearing in the measured spectrum. A diagram demonstrating this sequence of decay processes following a heavy-ion compound nuclear reaction is shown in Figure III-2.[26] Consequently, this decay process selectively populates yrast and near-yrast states, thus placing qualitative limits on the angular momentum values of observed states.

B. Gamma-ray Excitation Measurements

Excitation measurements involve determining the intensity of each gamma-ray as a function of incident beam energy. These intensities should follow a very similar pattern to that of the cross-sections shown in Figure III-1, thus allowing identification of gamma-rays belonging to a given final nucleus. In addition, the intensity curve for a given gamma-ray also contains a dependence on the angular momentum of the deexciting state. This is because a higher energy incoming beam on the average leaves the residual nucleus with more angular momentum, which results in the population of higher-spin states.

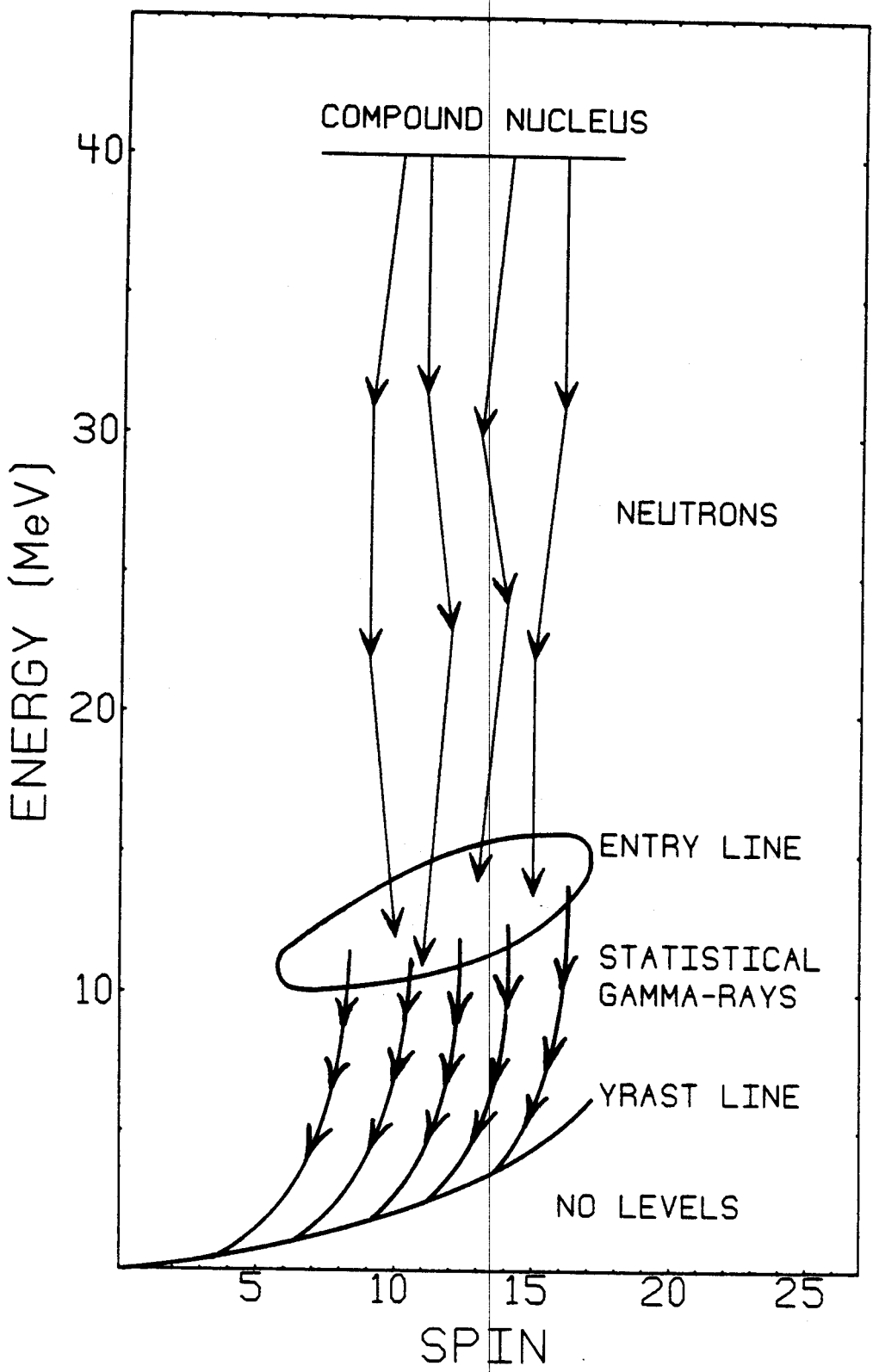

Figure III-2 Schematic illustration of the decay of a compound nucleus in a (HI,3n) reaction

Therefore, information on the relative spin values of different states can be obtained from this type of experiment.

C. Gamma-ray Angular Distributions

The large amount of orbital angular momentum brought into the compound system by the projectile is oriented in a plane perpendicular to the beam direction. Using this beam direction as a quantization axis, it follows that the high-spin states will have their angular momentum preferentially aligned in low-m substates. This alignment is greatest for high-lying states and slowly diminishes as the nucleus decays down to lower-lying levels.

Because of the alignment, the probability for a decaying gamma-ray to be emitted is not isotropic. When the intensity of a gamma-ray is measured with respect to the beam direction, it displays an angular dependence, the shape of which is determined by the spins of the initial and final states, the multipolarity mixing of the transition, and the degree of alignment of the initial state. The angular dependence can be expressed as an expansion of even Legendre polynomials as shown in the following equation:

$$I(\theta) = A_o + A_2 P_2 (\cos\theta) + A_4 P_4 (\cos\theta)$$
$$= I_o \{1 + \alpha_2 A_2'/A_o P_2 (\cos\theta) + \alpha_4 A_4'/A_o P_4 (\cos\theta)\}$$

The experimental intensities for each gamma-ray are fit to this equation and the $\alpha_2 A_2'/A_o$ and $\alpha_4 A_4'/A_o$ coefficients are extracted, as well as the integrated intensity I_o. Once

the alignment attenuation coefficients α_2 and α_4 have been determined, the resulting A_2'/A_o and A_4'/A_o coefficients can then be compared with calculated values to obtain information on the allowable spin values of the levels involved.

Values for the attenuation coefficient α_2 can be determined experimentally if the nucleus exhibits several pure multipolarity transitions. In deformed nuclei such transitions occur frequently as electric quadrupole I→I-2 transitions in rotational bands. In the case of ^{116}Sb, using the $(\alpha,3n\gamma)$ reaction, several such pure transitions were excited. Figure III-3 shows a plot of the attenuation parameter α_2 determined from these transitions. It can be seen from the figure that over the range of interest α_2 is quite insensitive with respect to the angular momentum of the individual states. For this reason α_2 was assumed to have the same value, 0.8±0.1, for all of the transitions considered in this experiment.

An experimental determination of α_4 is quite unreliable. However, making some simple assumptions about the shape of the m-substate population allows α_4 to be calculated from α_2.[27] Using this method α_4 for this experiment was determined to be 0.5±0.1.

Once the attenuation coefficients are determined, comparisons with calculated results[27] can be made. Figure III-4 shows a plot of calculated angular distribution coefficients. The alignment parameters discussed above have already been folded in, so that this plot may be compared

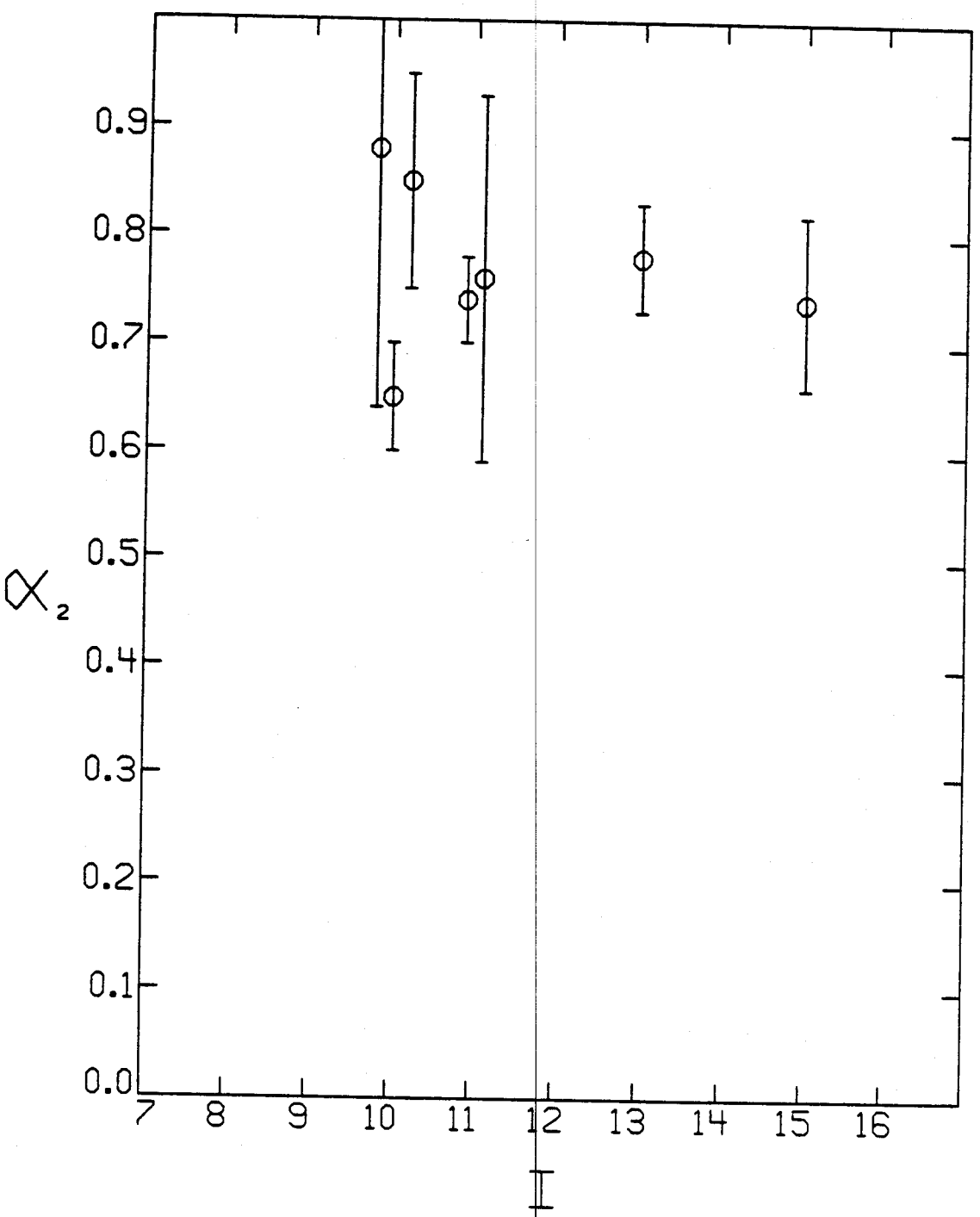

Figure III-3 The spin alignment attenuation coefficient α_2 as a function of spin for pure multipolarity transitions in ^{116}Sb

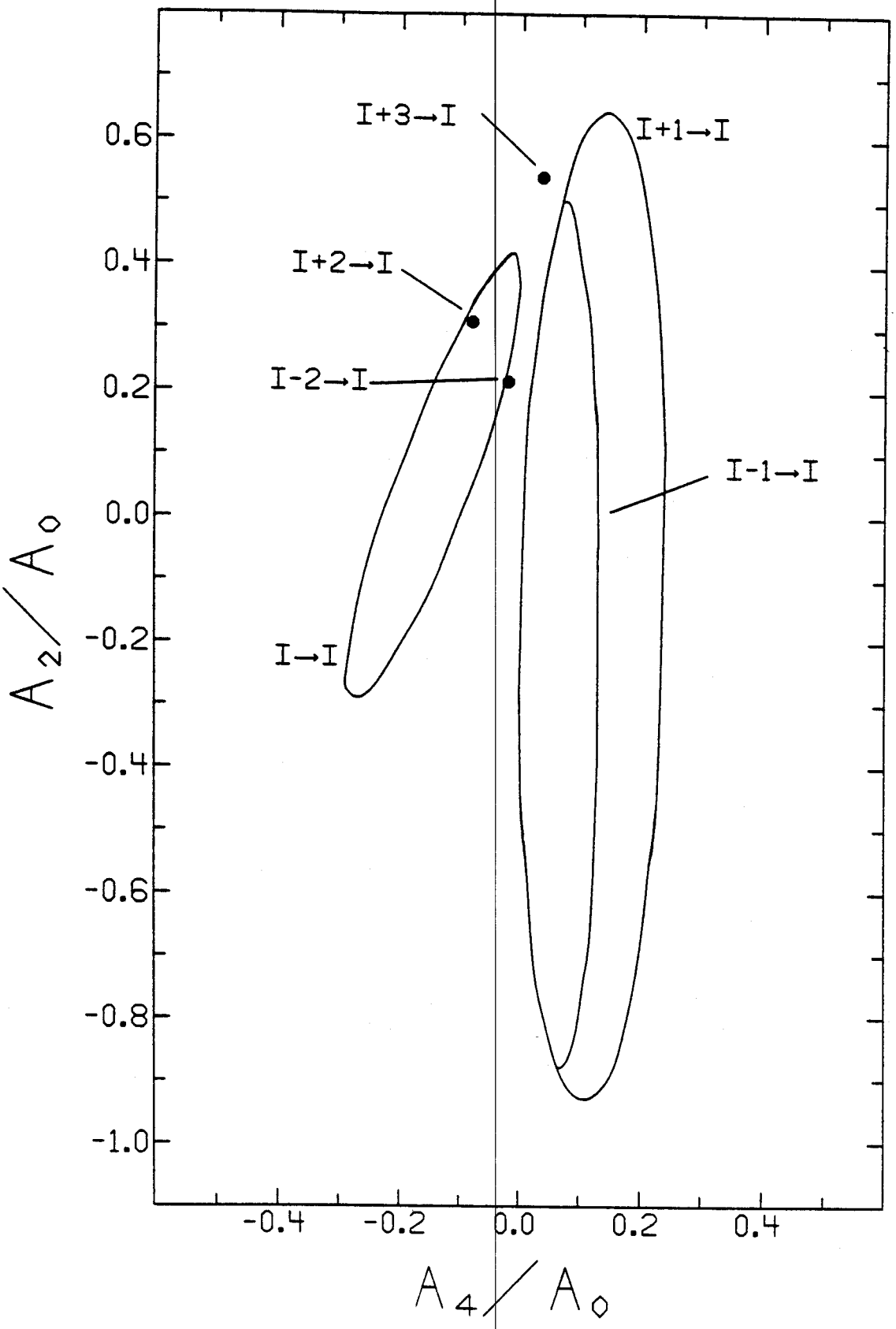

Figure III-4 The angular distribution coefficients A_2/A_0 and A_4/A_0 for transitions to states with spin $I_f = 8$

directly with the experimentally determined coefficients. Each ellipse corresponds to transitions with different $I_i \rightarrow I_f$ values, while each point on an ellipse corresponds to a different value for δ, the multipolarity mixing ratio. Since mixed high multipolarity transitions are in general quite rare, only single points corresponding to $\delta=0$ are shown for the $\Delta I=2$ and $\Delta I=3$ transitions. The plots shown here correspond to transitions with $I_f = 8$. Since these curves change only slightly with different values of I_f, they may be used to determined allowable spin values for any of the high spin states. However, in order to get a quantitatively correct value for the mixing ratio δ, the theoretical curves corresponding to the correct final spin must be used.

For the case of ^{118}Sb, a (p,3nγ) reaction was used in performing the angular distribution experiment. This reaction does not leave the final nucleus with too much angular momentum and consequently insufficient information is available to determine accurately the attenuation coefficients. They should however, not be too different from those determined in the (α,3nγ) reaction. Because of this, only a qualitative determination of the mixing ratios can be made from this experiment.

In addition to determining possible spin values, angular distribution results can also in some cases be used to establish parity assignments. This is because the transition probability varies widely for different multipolarity

transitions. Thus while M1 and E2 multipolarities mix quite readily, E1 and M2 multipolarities have such differing transition rates they do not mix. Consequently the observation of a large amount of mixing in a dipole-quadrupole transition, will establish it as an M1/E2 transition. A similar argument can be applied to pure quadrupole transitions. Because the transition probability for M2 transitions has such a small value, they occur only with long half-lives. Thus the observation of a pure quadrupole transition without a significant half-life will establish it as an E2 transition.

D. γ-γ-t Coincidence Measurements

Normally the lifetimes of most nuclear states are much less than a nanosecond. Therefore, after a single compound nuclear reaction, many gamma-rays will be emitted within a very short time period. These gamma-rays then compose one possible decay sequence of the excited final nucleus. By detecting multiple gamma-rays resulting from a single nuclear reaction event, it is possible to reconstruct the decay sequence which produced them and thus determine the excitation energies of the excited states.

Coincidence experiments were performed for both ^{116,118}Sb. The energies of two gamma-rays from two detectors along with the time interval between their detection were collected and recorded event by event onto magnetic tape. Following each experiment, gates were set on a specific gamma-ray energy from one detector and a specific time interval. A projected spectrum from the other detector is produced by collecting

all events with the first two parameters occuring within the gated regions. The gamma-ray peaks which occur in this spectrum are then known to be in coincidence with the gated gamma-ray.

E. Gamma-ray Half-life Measurement

Although most excited nuclear states decay very quickly, occasionally there occurs a state which is unable to decay by magnetic dipole or electric quadrupole transitions. These states will probably have measurable half-lives. High multipolarity transitions have intrinsically long half-lives, while electric dipole transtions often involve unique-parity single-particle orbitals which lead to ℓ-forbiddeness, thus slowing their decay.

The most straight forward method for measuring a nuclear half-life requires a pulsed accelerator beam. The M.S.U. cyclotron is ideal for this, because it delivers particles in well defined pulses. In addition, to increase the available time between pulses, a beam sweeper may be used to select periodic cyclotron beam bursts. With this device half-lives from about 1 nsec to approximately 1 μsec can be measured.

A half-life experiment involves collecting gamma-ray energies in coincidence with a time signal, which denotes when the gamma-ray occured relative to a beam burst. The gamma-ray is then placed in one of 10 spectra depending on the value of the time parameter. Analysis of the data then involves determining the intensity of the delayed gamma-ray

from each spectra. These intensities can then be plotted against the corresponding time parameter, thus determining the half-life.

IV. ^{116}Sb EXPERIMENTAL RESULTS

A. Experimental Arrangement

High-spin states of ^{116}Sb were populated using the ^{115}In(α,3nγ)^{116}Sb reaction. The beams were supplied by the M.S.U. Cyclotron. The target used was a natural, metallic indium foil of about 1 mg-cm^{-2} thickness. This was acceptable because ^{115}In has a natural isotopic abundance of 95.7%. The measurements were performed using Ge(Li) detectors, standard electronics, and a Sigma-7 computer for data acquisition. The same computer along with the peak fitting code SAMPO[28] was used for off-line analysis of the spectra.

A singles spectrum of ^{116}Sb is shown in Figure IV-1. This spectrum was obtained using a beam energy of 42 MeV with a detector angle of 130°. As indicated in this figure, in addition to the gamma-rays associated with the high-spin states of ^{116}Sb, many gamma-rays appear which belong to various neighboring nuclei. These result from the competition of the (α,2nγ) and (α,4nγ) reactions, which produce ^{117}Sb and ^{115}Sb respectively. These two nuclei, along with ^{116}Sb, beta decay with half-lives ranging from 31 to 168 minutes, resulting in the appearance of gamma-rays belonging to the daughter nuclei ^{115,116,117}Sn. In addition, several of the gamma-rays labeled ^{116}Sb are associated with the previously studied,[3] low-lying, low-spin levels of this nucleus. Since the present study contains no new or contradictory information with respect to existing results concerning

Figure IV-1 Spectrum of ^{115}In (α,3nγ) obtained at 130° with respect to the beam

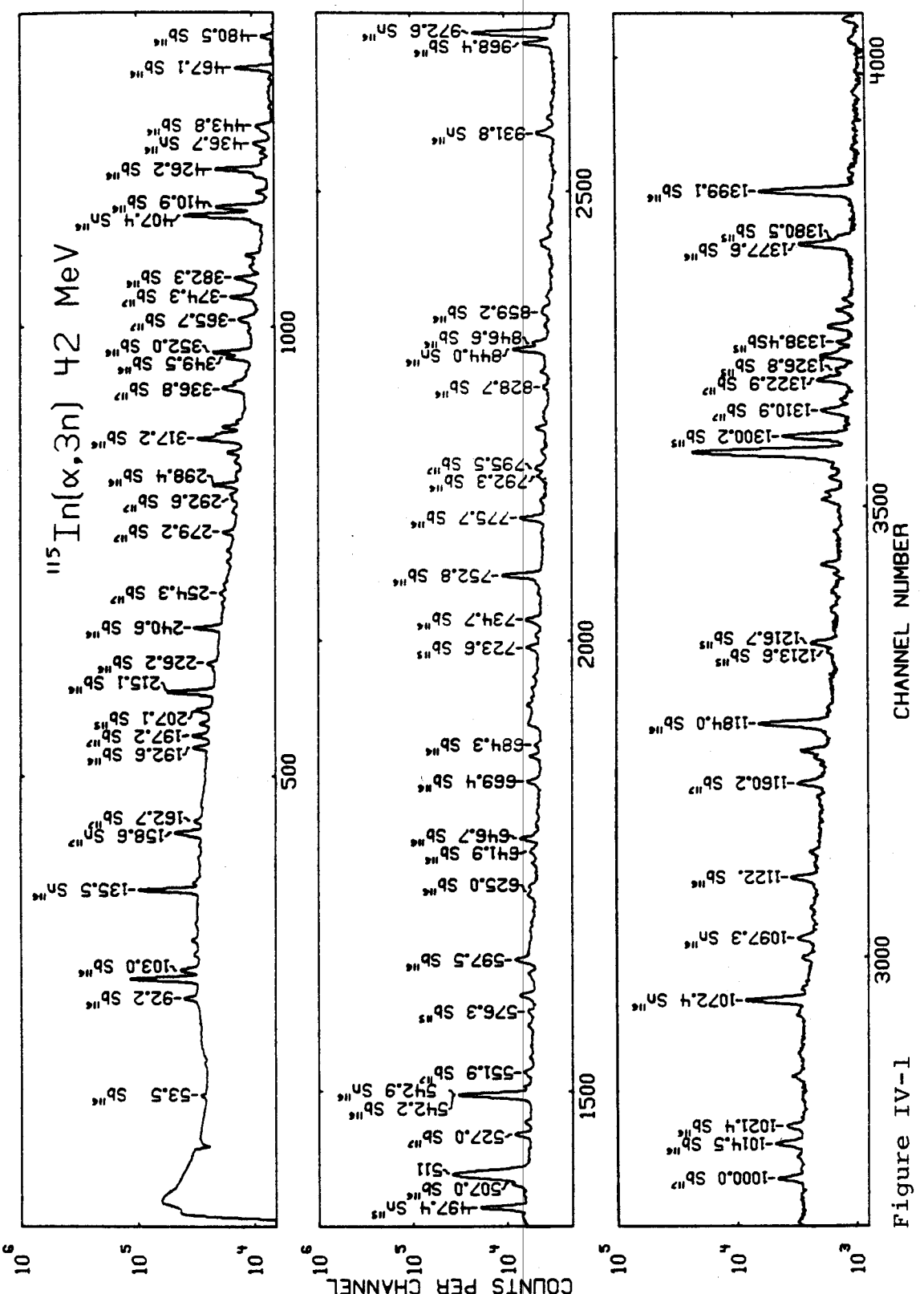
^{115}In(α,3n) 42 MeV
COUNTS PER CHANNEL
CHANNEL NUMBER
-53.5 Sb^{116}
-92.2 Sb^{116}
-103.0 Sb^{116}
-135.5 Sn^{116}
-158.6 Sn^{117}
-162.7 Sb^{117}
-192.6 Sb^{116}
-197.2 Sb^{117}
-207.1 Sb^{115}
-215.1 Sb^{116}
-226.2 Sb^{116}
-240.6 Sb^{116}
-254.3 Sb^{117}
-279.2 Sb^{117}
-292.6 Sb^{117}
-298.4 Sb^{116}
-317.2 Sb^{116}
-336.8 Sb^{117}
-349.5 Sb^{116}
-352.0 Sb^{116}
-365.7 Sb^{117}
-374.3 Sb^{117}
-382.3 Sb^{116}
-407.4 Sn^{116}
-410.9 Sb^{116}
-426.2 Sb^{116}
-436.7 Sn^{116}
-443.8 Sb^{116}
-467.1 Sb^{116}
-480.5 Sb^{116}
-497.4 Sn^{115}
-507.0 Sb^{116}
-511
-527.0 Sb^{117}
-542.2 Sb^{116}
-542.9 Sn^{116}
-551.9 Sb^{117}
-576.3 Sb^{115}
-597.5 Sb^{116}
-625.0 Sb^{116}
-641.9 Sb^{116}
-646.7 Sb^{116}
-669.4 Sb^{116}
-684.3 Sb^{116}
-723.6 Sb^{115}
-734.7 Sb^{116}
-752.8 Sb^{116}
-775.7 Sb^{116}
-792.3 Sb^{116}
-795.5 Sb^{117}
-828.7 Sb^{116}
-844.0 Sn^{116}
-846.6 Sb^{116}
-859.2 Sb^{116}
-931.8 Sn^{116}
-968.4 Sb^{116}
-972.6 Sn^{116}
-1000.0 Sb^{117}
-1014.5 Sb^{116}
-1021.4 Sb^{116}
-1072.4 Sn^{116}
-1097.3 Sn^{116}
-1122. Sb^{116}
-1160.2 Sb^{117}
-1184.0 Sb^{116}
-1213.6 Sb^{115}
-1216.7 Sb^{115}
-1300.2 Sb^{115}
-1310.9 Sb^{117}
-1322.9 Sb^{117}
-1326.8 Sb^{115}
-1338.4Sb^{115}
-1377.6 Sb^{116}
-1380.5 Sb^{115}
-1399.1 Sb^{116}

Figure IV-1

these other nuclei and low-spin levels in ^{116}Sb, no further discussion or reference will be made with regard to these transitions, except to indicate where they interfere with transitions resulting from the decay of high-spin levels in ^{116}Sb.

An energy calibration was performed by simultaneously collecting gamma-rays from a standard radioactive source, ^{152}Eu. This was corroborated by the many known transitions in the spectra which provided a very good internal calibration.

B. Results of Gamma-ray Angular Distribution Measurement

An angular distribution experiment was performed using a 42 MeV alpha beam. The detector used was an 8% efficient coaxial Ge(Li) detector. An additional Si surface barrier detector was included for normalization between the different angles. It was positioned at a fixed angle of -45° and was used to detect elastically scattered alpha particles.

Gamma-ray spectra were collected at angles of 90°, 100°, 110°, 120°, 130°, 140°, 150°, and 155° chosen in a random order to minimize the possibility of systematic errors. At each angle data were accumulated for approximately two hours. Figure IV-2 shows some representative examples of the angular distributions that were obtained. A compilation of the results of the experiment is contained in Table IV-1. Included in this table are the experimentally determined angular distribution coefficients along with the relative integrated intensities Io. These

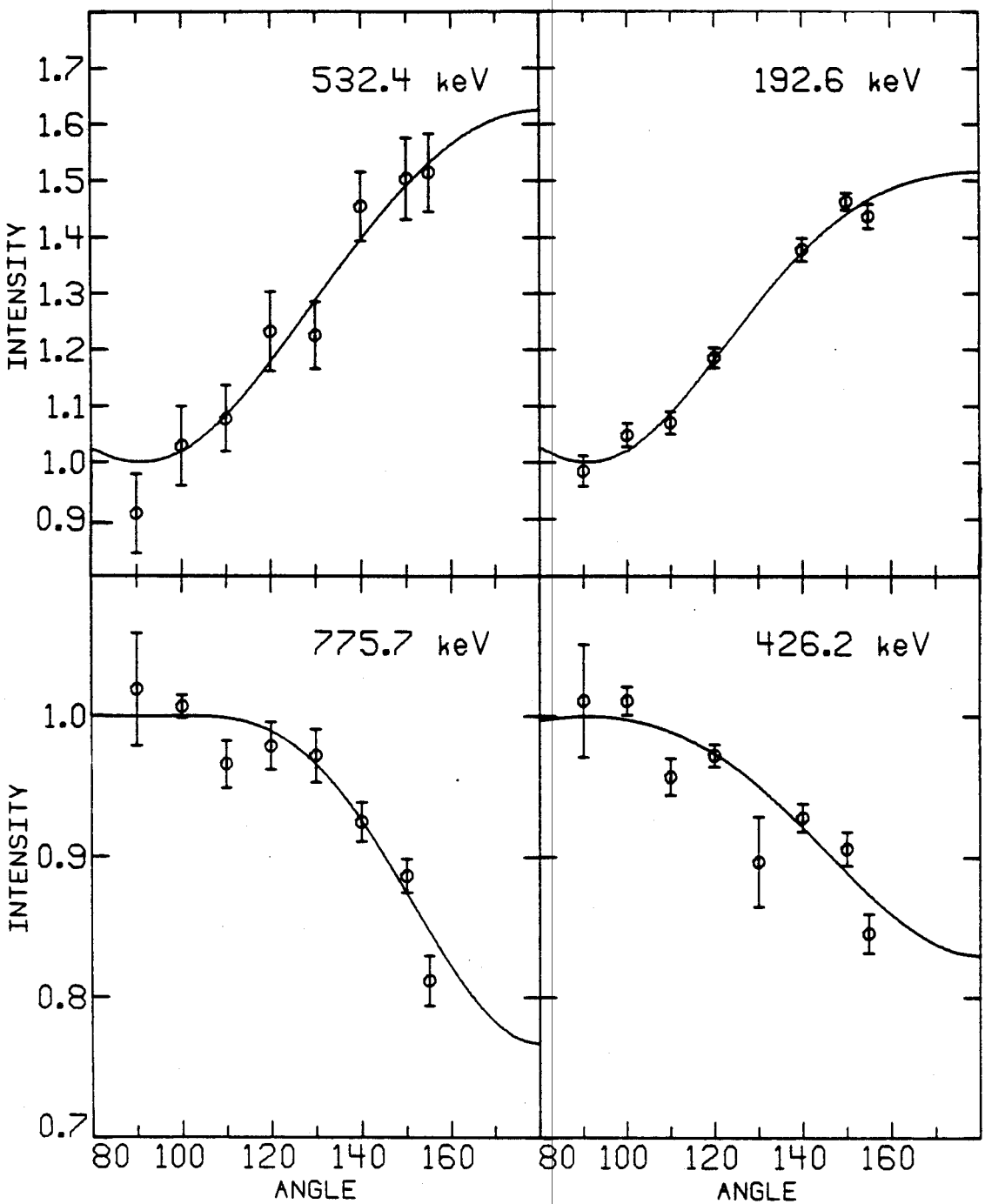

Figure IV-2 Angular distributions for selected ^{116}Sb transitions. The fits are normalized to 1 at 90°

Table IV-1 Energies (E_γ), Relative intensities (Io), angular distribution coefficients, multipolarities and spin assignments for transitions in ^{116}Sb.

E_γ[a] (keV)	Io[b] rel.	A_2/A_0	A_4/A_0	$I_i \rightarrow I_f$	δ
21.6[c]	1.7			11→10	
53.5	27.0	-0.15±0.05	0.09±0.08	7→8	
99.8[d]	41.5	-0.18±0.10		8→7	
121.8	2.5	0.11±0.04	0.28±0.07		
127.4	0.8	-0.41±0.12	0.00±0.25	7→8	
142.2[c]	0.7				
192.6	11.8	0.31±0.02	-0.06±0.04	7→7	
215.1	50.6	-0.07±0.02	-0.02±0.06	9→8	$0.18<\delta<0.21$
226.2	8.1	-0.91±0.02	0.08±0.04	15→14	$-1.25<\delta<-0.68$
240.6	23.0	0.63±0.03	0.22±0.05	14→13	$0.86<\delta<1.37$
298.4	18.3	0.04±0.03	-0.01±0.06	8→8	
317.2	41.1	-0.03±0.03	0.02±0.04	10→9	$0.10<\delta<0.14$

Table IV-1 (cont'd)

E_γ (a) (keV)	I_o (b) rel.	A_2/A_0	A_4/A_0	$I_i \rightarrow I_f$	δ
341.1 (e)	1.9	-0.30±0.09		(11)→10	
349.5	16.8	0.14±0.03	0.00±0.06	7→7	-0.55<δ<-0.41
352.0 (c)	27.2			(11)→10	
382.3	14.7	-0.07±0.03	0.01±0.04	(12)→(11)	0.07<δ<0.11
389.1 (c)	1.0				
404.9	6.8	0.19±0.06	0.00±0.11	(9)→(8)	0.24<δ<0.33
410.0 (c)	10.0			(13)→(12)	
410.9 (c)	21.4			(8)→7	
423.7	5.0	0.08±0.04	0.02±0.07	(10)→(9)	0.17<δ<0.23
426.2	47.3	-0.11±0.02	-0.02±0.04	7→8	-0.14<δ<-0.01
435.3 (c)	2.5			(11)→(10)	
443.8 (e)	7.1	0.03±0.07		(14)→(13)	0.11<δ<0.21

Table IV-1 (cont'd)

E_γ (a) (keV)	Io (b) rel.	A_2/A_0	A_4/A_0	$I_i \rightarrow I_f$	δ
467.1	27.6	0.29±0.03	-0.06±0.05	15→13	
480.0	7.5	-0.33±0.04	-0.08±0.05	(8)→7	
507.0 (c)	14.0				
532.4	3.9	0.35±0.04	-0.03±0.06	10→8	
542.2 (d)	8.1	0.50±0.30		7→7	
597.5 (e)	14.3	0.09±0.06			
625.0	3.5	-0.51±0.05	-0.10±0.07	10→9	
641.9	5.0	-0.07±0.03	0.01±0.06	8→7	$0.07<\delta<0.13$
646.7	14.3	0.41±0.02	-0.02±0.04	11→9	$0.07<\delta<0.13$
669.2 (c)	6.0			(11)→9	
669.4 (c)				(11)→(11)	
669.8 (c)	7.0			7→8	

Table IV-1 (cont'd)

E_γ (a) (keV)	Io (b) rel.	A_2/A_0	A_4/A_0	$I_i \rightarrow I_f$	δ
684.3 (e)	4.6	-0.47±0.08			
734.7 (c)	6.0			(12)→10	
752.8	58.3	-0.58±0.03	-0.03±0.06	9→8	-0.28<δ<-0.22
752.6 (c)	8.0				
775.7	25.1	-0.14±0.02	-0.06±0.04	7→8	-0.03<δ<0.01
792.3	4.6	0.44±0.09	-0.13±0.16	13→11	
828.7 (e)	3.1	0.36±0.10		(10)→(8)	
846.6	12.9	0.03±0.05	-0.04±0.08		
854.0 (c)	3.6			(14)→(12)	
859.2	5.6	0.31±0.07	-0.13±0.12	(11)→(9)	
906.1 (c)	2.9			(8)→(8)	
968.4	38.0	-0.26±0.02	-0.01±0.03	7→8	

Table IV-1 (cont'd)

E_γ (a) (keV)	I_o (b) rel.	A_2/A_0	A_4/A_0	$I_i \rightarrow I_f$	δ
1014.5	24.9	-0.09±0.03	0.01±0.04	8→7	
1021.4	13.9	-0.18±0.03		(11)→10	
1110.2 (e)	3.3	-0.31±0.12			
1122.0	18.9	-0.75±0.02	0.07±0.04	(13)→(12)	
1184.0	70.5	0.31±0.02	-0.09±0.03	13→11	
1283.2	6.0	-0.47±0.07	-0.06±0.11	9→8	$-0.21<\delta<-0.10$
1377.6	33.0	0.27±0.02	-0.09±0.03	10→8	
1399.1	100.0	0.53±0.02	0.05±0.04	11→8	
1504.3 (c)				(13)→(11)	

a) Energy uncertainties are 0.2 keV for most transitions, rising to 0.5 keV for weak transitions and components of multiplets.

b) Intensity uncertainties are approximately 15% for most transitions, rising to 30% for weak transitions and components of multiplets.

c) These are transitions which are too weak to fit or are components of unresolvable multiplets.

d) Coefficients for these transitions were obtained by subtracting appropriate amount of interfering ^{116}Sn peak calculated from known intensity ratios.

e) These are weak transitions for which A_4 was set to zero during the fitting procedure.

intensities have been corrected for detector efficiency and normalized such that the 1399-keV transition, the most intense transition appearing in the level scheme, has the value 100. It should be noted that except for the 22-keV transition which will be discussed later, no attempt was made to correct for conversion intensities. For those transitions which are part of unresolvable multiplets, estimates of the intensity have been made from the coincidence experiment, where possible. The table also includes the proposed spin values of the initial and final states associated with each transition, as well as the multipole mixing ratio.

C. Results of γ-γ-t Coincidence Experiment

The coincidence experiment was performed using a beam energy of 38 MeV. Two coaxial Ge(Li) detectors, each with an efficiency of approximately 9%, were placed at $\pm$ 90° with respect to the beam direction. Approximately 30×10^6 coincidence events were collected. Figure IV-3 shows several examples of the gated spectra. The results of this experiment are given in Table IV-2.

D. Results of Half-life Measurement

A half-life experiment was performed using a beam energy of 38 MeV. A high resolution intrinsic Ge detector was positioned at 90° with respect to the beam direction. Data were collected in 10 separate time spectra determined with respect to the cyclotron r.f. signal. A portion of these spectra showing the decay of the 426-, 753-, 647-,

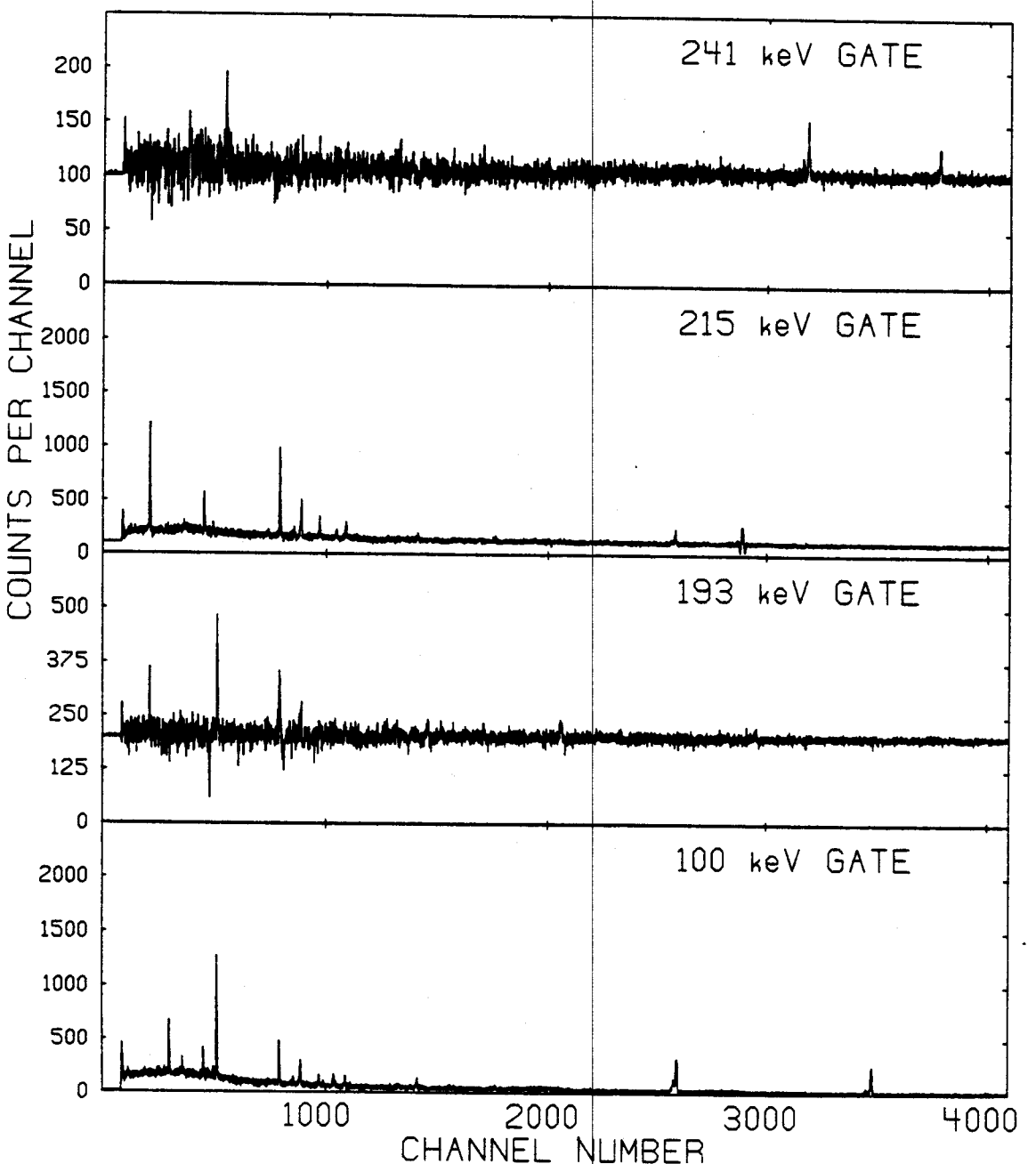

Figure IV-3 Background subtracted gated coincidence spectra for selected transitions in ^{116}Sb

Table IV-2 Results of γ-γ-t coincidence experiment for transitions in ^{116}Sb.

Gate Energy (keV)	Coincident Gamma-Rays (keV)
100[a]	136[a,e], 193, 215, (298), 317, 341, 352, 382, 389, 407[a,e], 410, 426, (444), 542[a], 776, 847, 968, 973[a,e], 1021, 1294[a,e]
193	100, (142), 215, 317, 350, 352, 382, 410, 426, (444), 562[e], 776
215[b]	100, 193, 207[b,e], 298, 317, 341, 352, 382, 389, 410, 426, 442[b,e], 444, 542, 669, (735), 776, (792), 968, (1021)
226	241, 507, 753, 1184
241	226, (507), 598, 1184, 1399
298	(127), (215), 350, 670
317	100, (133)[e], 193, 215, 294[e], 320[e], 341, 352, 382, 407[e], 410, 426, 542 (735), (776), 968, (1021)
341	100, 215, 317, 389
350[c]	100, 193, 197[c,e], 202[c,e], 215, 317, (352), (382), 411, 426, (527)[c,e], (1000)[c,e]
352[d]	100, 103[d,e], 157[d,e], 193, 215, 317, (341), (350), 382, 410, 426, 444, (532), (542), 776, (792), 968, (1283), 1504
382	100, 193, 215, 298, 317, 352, 405[e], 410, 426, 444, 669, (839)[e], (854), 968, (1122)
405[a]	92[e], 100[a,e], 136[a,e], 319[e], 381[e], 392[e], 411, 424, 426, 437[a,e], (467)[e], 776, (859), 973[a,e], 1072[a,e], 1294[a,e]

Table IV-2 (con't)

Gate Energy (keV)	Coincident Gamma-Rays (keV)
411[d]	92[d,e], 100, 215, 224[d,e], 317, 338[d,e], 352, 382, 392[e], 405[d], (411)[e], 424, 426, 435, 776, (829), (859), 968
424	(392)[e], 405, 411, 435, 529[e], (776)
426	100, 193, 215, 317, 341, 350, 352, 382, (405), 410, 411, (424), 480, 542, (642), 684
444	100, 215, 317, (352), (382), 410, (792)
467	507, 598, (753), 1184, 1399
480	426
507	(226), (753)
532	100, (215)[e], (240)[e], (255)[e], 352, 382, (410), (933)[e]
542[a]	100[a], 136[a,e], 215, (294)[e], 317, (382), 426, (582)[e], 973[a,e], 1072[a,e], 1294[a,e]
598	(241), (407)[e], (467), (1184), (1399)
647	241, 753, 1184
670	100, 215, (298), (317), (352), (382)
753	(241), (317), (624), 647, 1021
776	(100), 215, 317, (352), (405), 411
968	100, 215, 317, 352, 382, 410
1015	215, (317), (352)
1184	(226), 241, 331[e], 467, 507, (598), (753), (840)[e], (886)[e], 1399

Table IV-2 (con't)

Gate Energy (keV)	Coincident Gamma-Rays (keV)
1399	241, (336)[e], (392)[e], 467, 495[e], 598, 1184

a) A transition with this energy is known to occur in ^{116}Sn
b) as (a) but ^{115}Sb
c) as (a) but ^{117}Sb
d) as (a) but the low spin level scheme of ^{116}Sb
e) These transitions have not been placed in the level scheme

and 776- keV gamma-rays is shown in Figure IV-4. The difference between each spectrum corresponds to a time interval of 4.36±0.04 nsec. Half-lives were determined for 13 gamma-rays, involved in the decay of 6 long-lived levels. The results of these measurements are tabulated in Table IV-3.

A plot of intensity as a function of time for transitions depopulating three of the metastable states is shown in Figure IV-5. It should be noted in this figure that the 753-keV transition displays evidence for a longer half-life component along with the 4-nsec component associated with the decay of the 1624-keV level. This, coupled with the coincidence relationships between the 753-, 1021-, and 317-keV transitions, indicate the 753-keV transition is a doublet, with each component involved in the decay of different states.

The two metastable states which display half-lives in the 1 nsec region are at the lower limit of sensitivity for this type of measurement. The difficulty is compounded in the case of the 1293-keV level by doublets and feeding from the higher lying 6-nsec states. Consequently, these two half-life values are associated with relatively large uncertainties.

E. Results of Excitation Function Measurement

In addition to the above experiments, which resulted in the excitation of high-spin states, an excitation function measurement was performed using a (p,4nγ) reaction at 37.8,

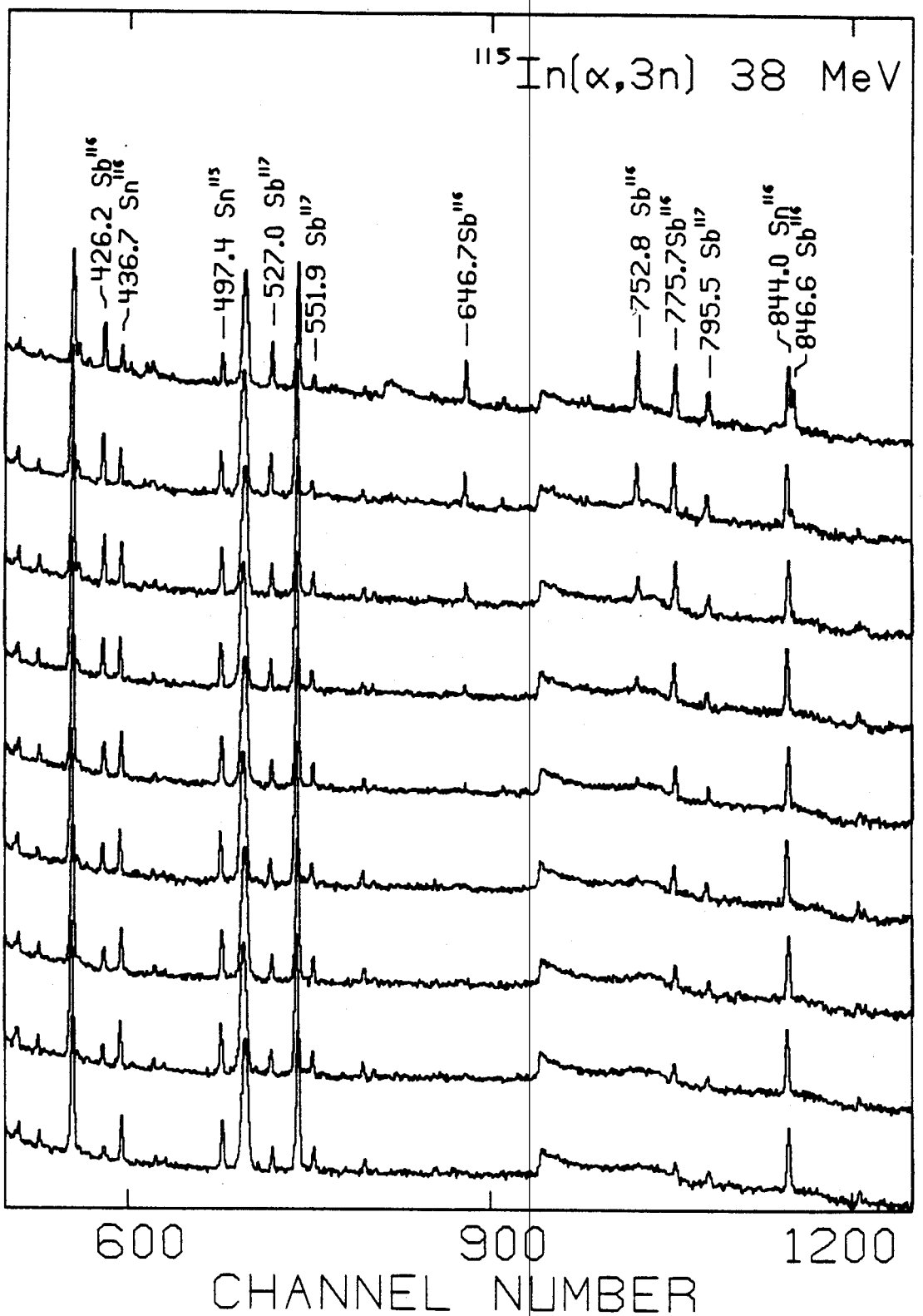

Figure IV-4 Delayed spectra from the $^{115}In(\alpha,3n\gamma)$ reaction. Delay time increases with each spectrum from top to bottom

Table IV-3 Half-lives determined for transitions involved in the decay of metastable states in ^{116}Sb

Metastable Level Energy (keV)	Transition Energy (keV)	Half-Life (nsec)
1001		12.6±0.2
	776	12.77±0.21
	426	12.33±0.22
1072		2.4±0.2
	847	2.42±0.20
1624		4.09±0.06
	1399	4.11±0.07
	1377	4.02±0.17
	753	4.30±0.10
	647	4.02±0.23
1193		1.0±0.5
	193	1.0±0.5
3049		1.3±0.4
	1184	1.4±0.5
	240	1.2±0.5
3599		7.1±0.2
	1021	7.74±1.16
	317	6.56±0.54
	215	7.16±0.23

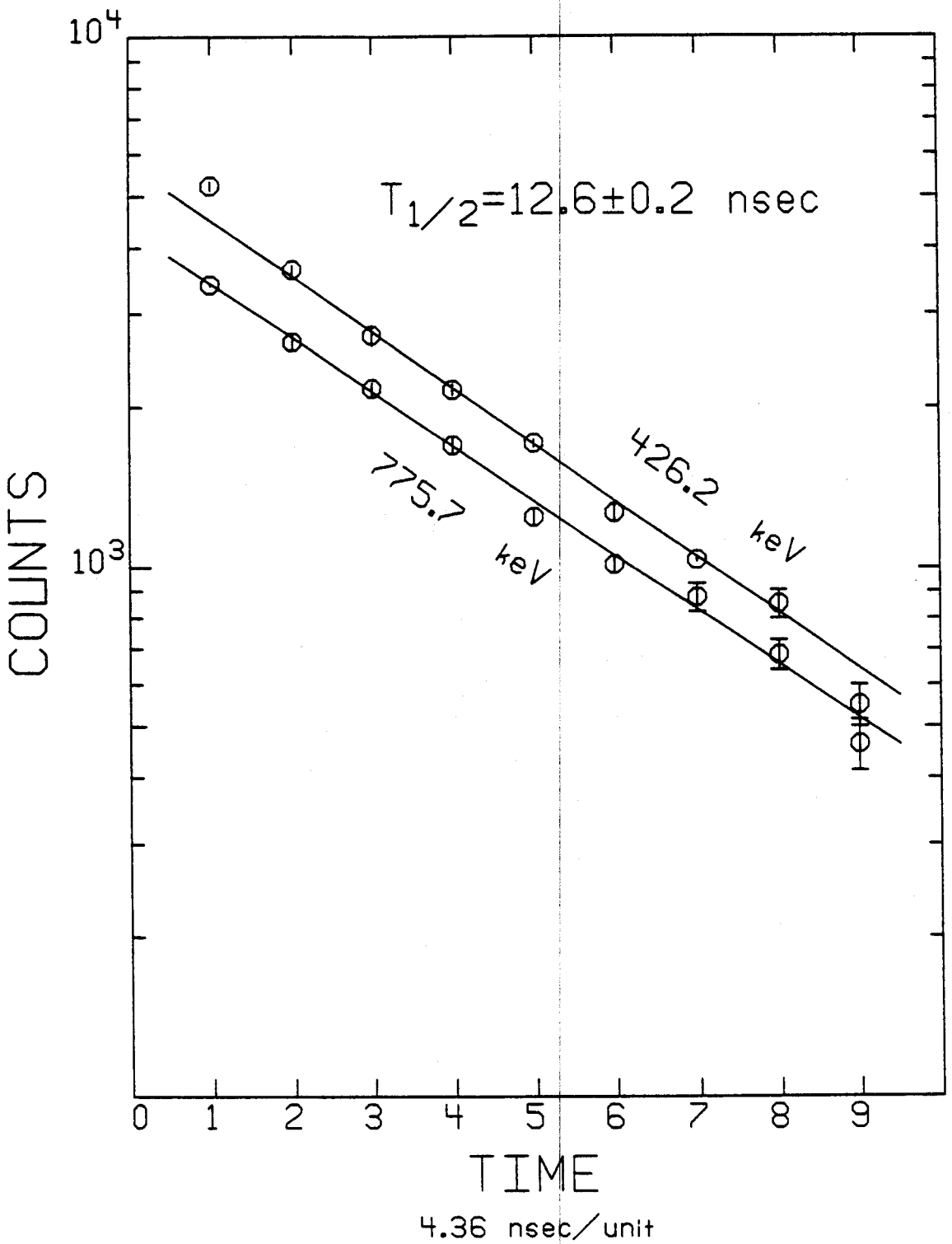

Figure IV-5a Half-life data for transitions occurring in the decay of the isomer at 1001 keV

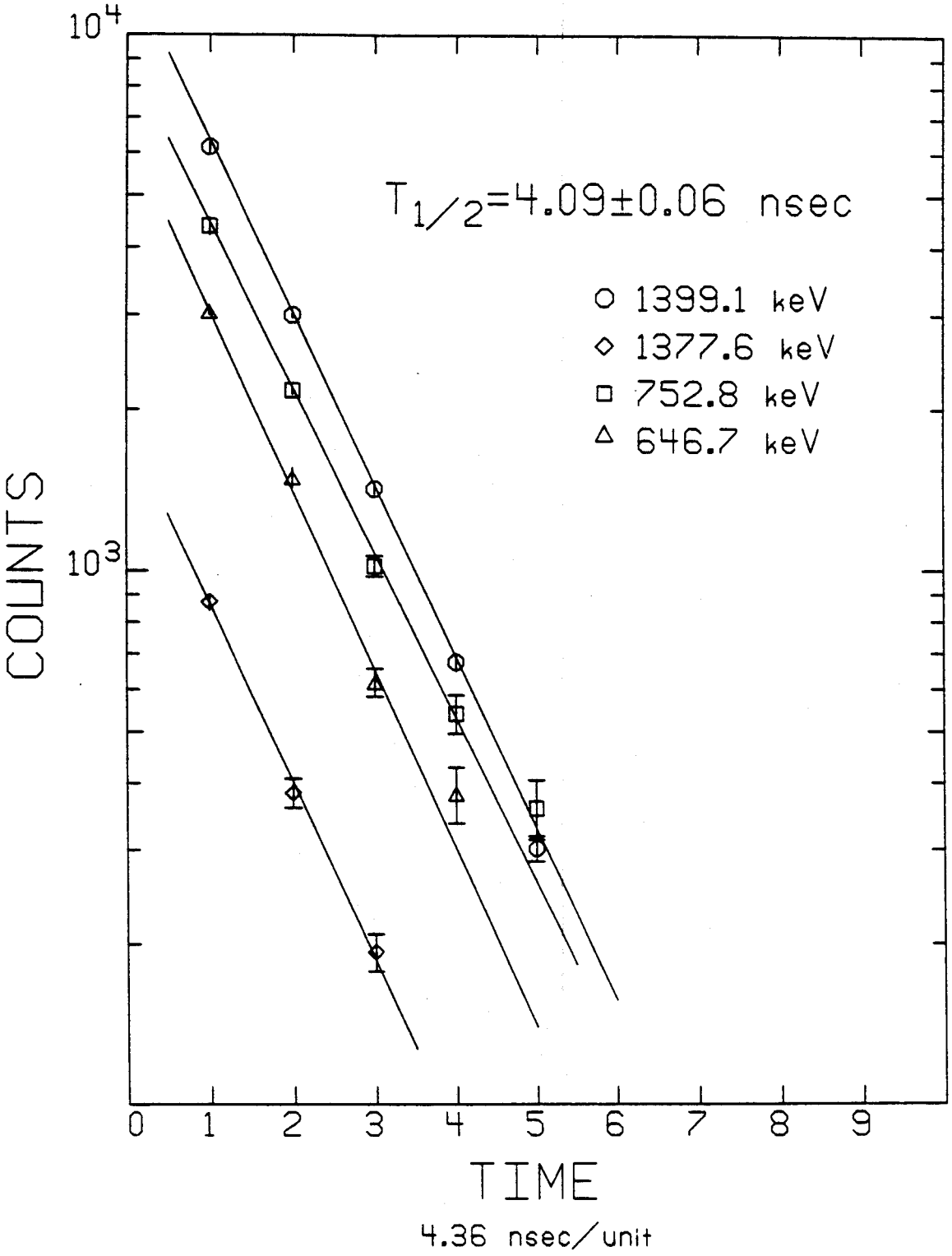

Figure IV-5b Half-life data for transitions occurring in the decay of the isomer at 1624 keV

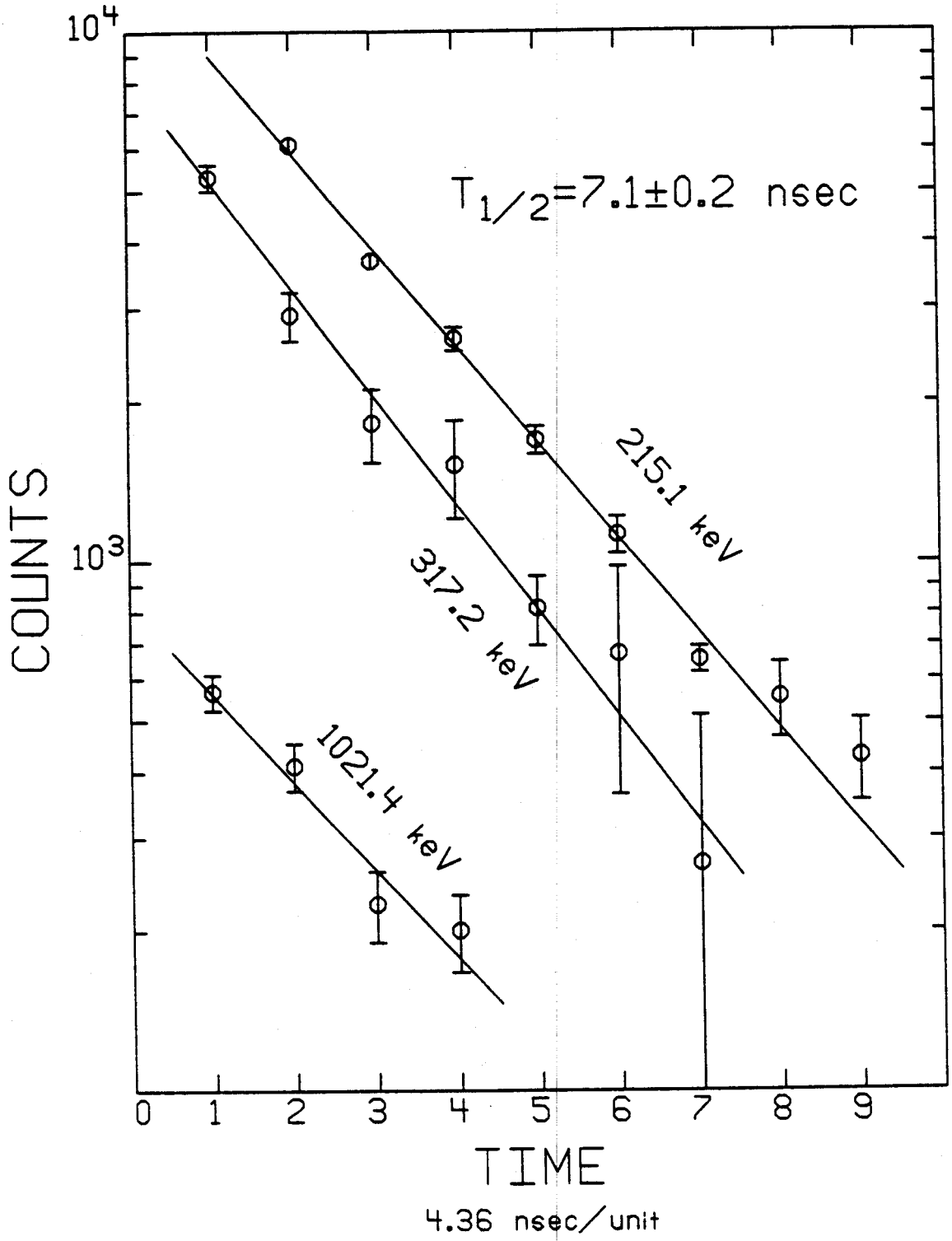

Figure IV-5c Half-life data for transitions occurring in the decay of the isomer at 3599 keV

40.0 and 44.0 MeV. These reactions were able to excite intermediate spin levels. The target used was an isotopically enriched ^{119}Sn metallic foil. The exact isotopic composition is unknown. However, from the results of the experiment it is evident that the percentage of ^{119}Sn is less than 50%. The remainder of the target is predominantly ^{120}Sn and ^{122}Sn.

Levels with spin to approximately 11ħ were excited. Because of the impurities in the target and the low intensity of most of the gamma-rays of interest, results for only 9 of the most intense gamma-rays were obtained from this experiment. These are shown in Figure IV-6.

F. ^{116}Sb Level Scheme

Identification of those gamma-rays associated with the decay of high-spin levels in ^{116}Sb first involves elmination of those gamma-rays associated with other nuclei. The remaining most intense gamma-rays can then be checked for consistent excitation function behavior. This establishes the lower-lying transitions in the level scheme. The coincidence experiment then identifies the less intense and higher-lying transitions, as well as those which form doublets with transitions in neighboring nuclei.

Once the gamma-rays belonging to ^{116}Sb have been identified, they may be arranged into a self-consistent level scheme. This is done by requiring that energy sum and coincidence relationships are satisfied and that the total intensity leaving each level is greater than that

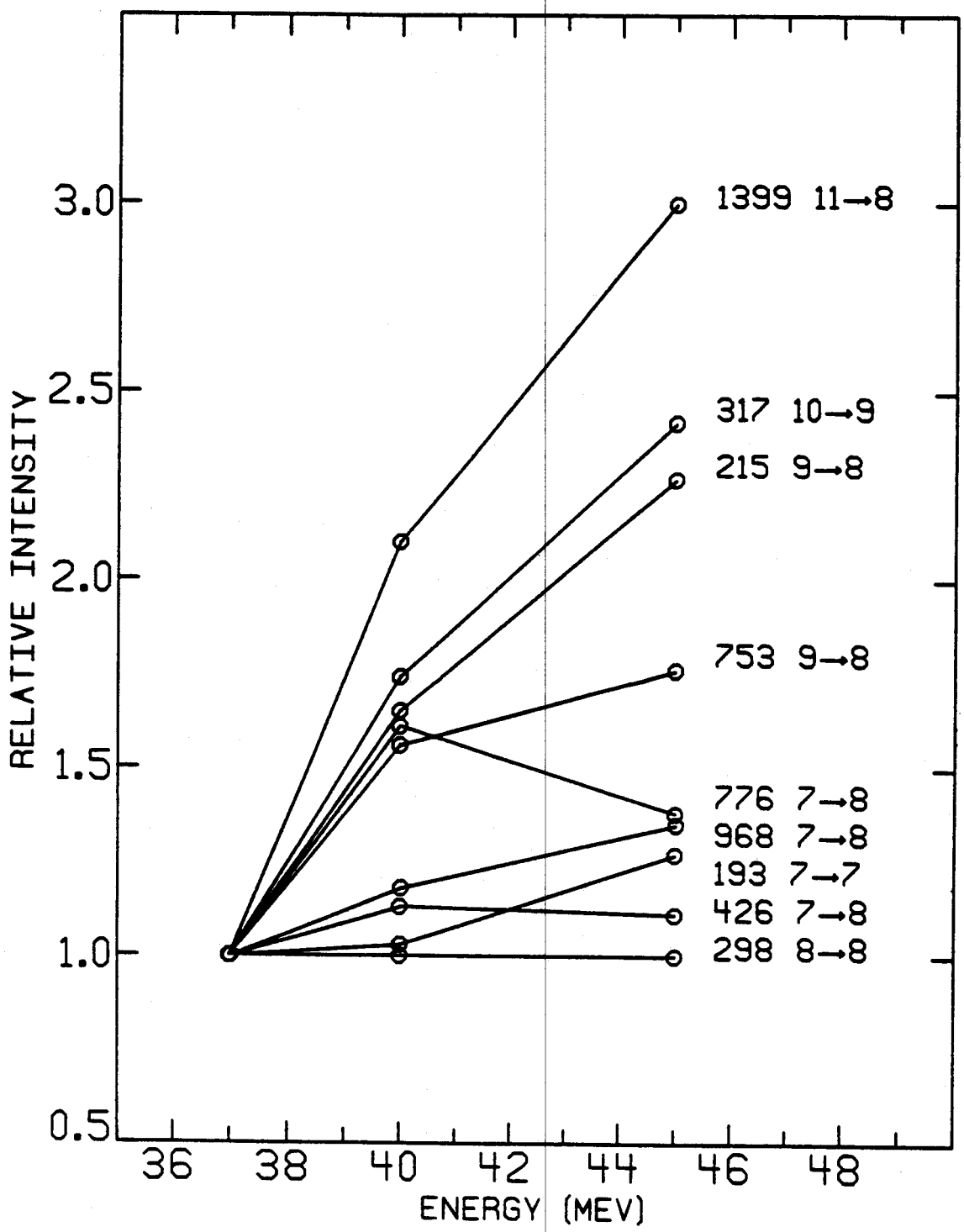

Figure IV-6 Excitation functions for selected transitions occurring in ^{116}Sb

which is entering. Applying these considerations to the gamma-rays associated with ^{116}Sb results in the level scheme shown in Figure IV-7.

The placement of most of the transitions is well established by the various experiments and consequently, will not be discussed. There are, however, a few cases where problems arise and these will now be discussed in detail. In particular, this level scheme exhibits a large number of gamma-rays which are part of multiplets. This can easily be seen in Table IV-1 where the multiple coincidence relationships are evident. The large number of multiplets lead to several difficulties in obtaining accurate energies, intensities and angular distribution coefficients. The most serious problem this caused was in the construction of the band built on the 1001 keV level.

1. The I=7 Band at 1001 keV

For this band all of the transitions are relatively weak components of multiplets. Explicitly, the 411-keV transition is part of a triplet, the other components being the 410-keV transition placed at 2970 keV and a 411-keV transition placed in the low-spin states of ^{116}Sb.[3] The 405-keV transition is part of a triplet with a very intense 407-keV transition in ^{116}Sn[29] and a very weak 404-keV transition from the low-spin states of ^{116}Sb.[3] The 424-keV transition is part of a triplet with an intense 426-keV transition placed at 651-keV in the level scheme and a weak 424-keV transition from the low-spin states of ^{116}Sb.[3]

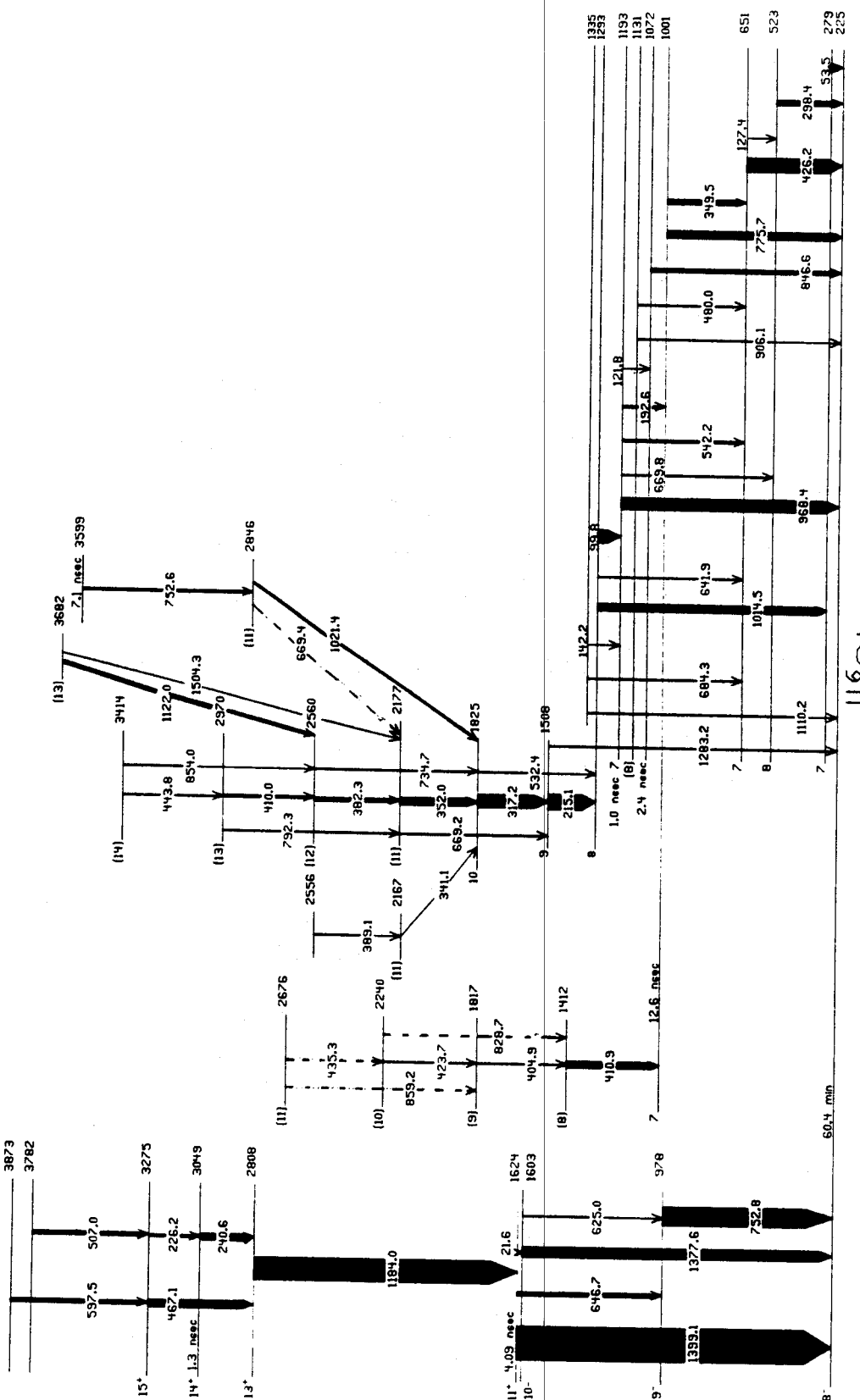

Figure IV-7 High-spin level scheme for ^{116}Sb

The final transition with energy 435 keV is a doublet with a very intense 437-keV transition in ^{116}Sn.[29] In addition, the two Sn transitions at 437 and 407 keV have a very strong coincidence relationship with each other, thus masking any possibility of seeing the 435- and 405-kev transitions in coincidence. Consequently, this makes the construction of the band very difficult.

Because of these problems the 435-keV transition is only tentatively placed as the highest transition in this band. In addition, because of the relative uncertainties in intensities, the ordering of the 424- and 405-keV transitions cannot be determined unambiguously. The order is chosen as indicated in the figure to accommodate the placement of the two crossover transitions, for which there is some, although weak, coincidence evidence. The band constructed in this way displays problems with intensity balances; however, these are probably the result of inadequacies in the peak fitting of the multiplets involved.

As the above discussion indicates, there is little about this band that can be stated with experimental exactness. However, the construction of the band as shown gives results which are systematically consistent with those of ^{118}Sb and consequently are quite likely correct.

2. The 21.6-keV Transition

The 21.6 keV transition depopulating the 1624-keV level was not observed in any of the experiments. Its existence was established by the occurrence of a 4-nsec delayed

component for the 1377-keV transition. Its intensity was determined from the intensity ratio of the 1377-and 1399-keV transitions in the delayed spectra. The intensity contribution from conversion electrons was then subtracted, assuming the transition to be a pure E1.

3. The 3599-keV Level

The assignment of the 7-nsec half-life to the 3599-keV level was based primarily on coincidence data. The 1021-, 317-, and 215-keV gamma-rays all displayed prompt components in their decay, indicating they do not depopulate this level directly. Consequently the metastable state feeding them must lie somewhere above this cascade of transitions. The 753-keV transition is established in the coincidence experiment as the only transition lying above and in cascade with these gamma-rays. Because it is a weak component of a doublet with another delayed transition, it is not possible to determine a half-life for this transition. However, because there appears to be evidence for a longer component than the 4-nsec component resulting from the decay of the 1624-keV state, the 7-nsec half-life is assigned to the 3599-keV level, which the 753-keV transition depopulates.

4. The 2560-keV Level

The 1122-keV transition brings too much intensity into the 2560-keV level. This indicates that either this transition is a doublet or that there is an unassigned transition depopulating the 2560-keV level. There is no

conclusive evidence to indicate which of these alternatives is correct. The placements of the remainder of the transitions are well established by coincidence and energy relationships.

G. Spin and Parity Assignments

The spin and parity assignments were made primarily on the basis of the angular distribution results. However, the excitation function data and intensity information are used in resolving some of the remaining ambiguities. It should be noted that most of the suggested spin assignments are not rigorously proven. They are based on many interdependent arguments and assumptions concerning how high-spin states decay. These assumptions are well established and generally give correct results. In this case they lead to a self-consistent set of spin assignments which can be explained in terms of the systematics of neighboring nuclei. The following is a discussion of some of the specific spin and parity assignments. For convenience of discussion the transitions and levels will be divided into groups.

1. The 8^- Metastable State

All of the spin and parity assignments depend upon the spin and parity of the lowest level in the scheme. The spin and parity for this level must be determined absolutely by an alternative means. For the lowest level depicted in Figure IV-7, there are two possibilities in ^{116}Sb, known from previous studies. These are the 16-minute 3^+ ground state and the 60.4-minute 8^- metastable state located at

225±60 keV. The latter of these two is the only reasonable alternative. Several reasons for this may be given. The most convincing of these is the appearance in the ^{115}In $(\alpha,3n\gamma)$ reaction of several very intense ^{116}Sn gamma-rays, which result only from the beta decay of the 8^- metastable state. This implies that a very large percentage of the intensity excited by this reaction must decay through this state. Previous studies of this level have included a determination of the spin[30] by use of the atomic beam method and a level energy determination[31], using the results of a beta decay study[32]. The values from these studies have been adopted here.

2. High-Spin Sequence

This section will discuss those levels which depopulate to the 8^- metastable state through the 1399-, 1378- or 753-keV transitions. This sequence of transitions is depicted on the left in Figure IV-7. The most precise angular distributions were obtained for this sequence of transitions. This is because they carry a very large percentage of the total intensity. This would tend to support the association of these levels with members of the yrast sequence. At the least, the large intensities imply increasing spin values with energy. This is also supported by the excitation function results which show the 753- and 1399-keV transitions displaying somewhat steeper slopes than the other low-lying transitions. Consequently this sequence will be referred to as the high-spin sequence.

The 753 keV transition which depopulates the 978-keV level displays a large negative A_2 coefficient indicative of a $\Delta I=1$ dipole transition. This results in an assignment of I=9 for the 978-keV level. In addition, the significant non-zero mixing ratio displayed by this angular distribution, requires this transition to have mixed M1/E2 character. Thus, the 978-keV level is assigned $I^{\pi}=9^{-}$.

Similarly the 625-keV transition from the 1603-keV level displays mixed M1/E2 character. The 1378-keV transition depopulating the same level displays a characteristic stretched E2 angular distribution. These results lead to the assignment of $I^{\pi}=10^{-}$ for the 1603-keV level.

The 1624-keV level has two transitions which depopulate it. One of these, the 1399-keV transition, has an angular distribution which exhibits a very large positive A_2 value. It can be associated with either a M1/E2 transition or a $\Delta I=3$ transition. Similarly, the 647-keV transition is consistent with either a dipole or a slightly mixed M2/E3, $\Delta I=2$ transition. This results in two possible assignments consistent with the angular distribution data. These are $I^{\pi}=9^{-}$ or 11^{+}. The excitation function measurement results, as well as the large intensities displayed by these transitions, support the higher spin assignment. In addition to these considerations, the $I^{\pi}=11^{+}$ assignment would require the 1399-keV transition to have E3 multipolarity. Such a high order multipolarity should result in an observable half-life for the 1624-keV level. A 4-nsec half-life was

determined experimentally for this level. Consequently the 1624-keV level is assigned to have $I^{\pi}=11^{+}$. With this assignment there results a large enhancement factor over the Weisskopf single-particle estimate for the half-life of the 1399-keV E3 transition. This is not unreasonable, however, considering a similar E3 transition in the neighboring nucleus ^{115}Sb is similarly enhanced,[13] and the corresponding transition[10] in ^{117}Sb exhibits a larger enhancement.

The 2808-keV level is assigned $I^{\pi}=13^{+}$ on the basis of the 1184-keV transition's stretched E2 angular distribution. Similarly the 3049- and 3275-keV levels are assigned to have $I^{\pi}=14^{+}$ and 15^{+}, respectively, on the basis of the stretched E2 behavior of the 467-keV angular distribution and the mixed M1/E2 behavior of the 226- and 240-keV transitions. Evidence concerning spin assignments for higher lying levels in this sequence is rather inconclusive; consequently, no assignments are made.

3. Medium Spin Levels

This section will discuss those levels located below 1300 keV, excluding the 978-keV level, which was discussed in the previous section. These levels are shown on the right in the level scheme. As can be seen in the figure, several of these levels decay to the 8^{-} metastable state. Of these transitions, four clearly display the angular distribution characteristics of $\Delta I=1$ dipole transitions. These are the 54-, 426-, 776-, and 968-keV transitions. The

corresponding levels which they depopulate must then have spin values of either I=7 or 9. The excitation measurements and intensity considerations suggest the lower spin value for these levels. This is also supported by the lack of any measurable intensity into any of these levels from the $I^{\pi}=11^{+}$ 1624-keV level. Consequently I=7 assignments are made for these four levels. There is no evidence for parity assignments.

The 523-keV level has a spin value of either 6 or 8 because of the $\Delta I=1$ dipole nature of the 127-keV transition. The near isotropic angular distribution of the 298-keV transition, which depopulates this level, eliminates the I=6 possibility. Therefore, the 523-keV level is assigned as having I=8.

A tentative assignment of I=8 is made for the 1131-keV level based on the angular distribution data for the 480-keV transition. Also the 1293-keV level is assigned as having I=8 on the basis of three $\Delta I=1$ dipole transitions from it to levels with I=7.

4. The I=7 Band

This band is built on the 1001-keV level, which has spin value I=7, as discussed above. Because this band was only weakly populated and most of the transitions are parts of multiplets, the angular distribution results for these transitions are subject to substantial systematic errors. However, the two tentatively placed crossover transitions display stretched E2 angular distribution characteristics

and the cascade transitions display consistent M1/E2 behavior. Consequently, this band is tentatively assigned spin values increasing by $\Delta I=1$ with each level.

5. The I=8 Band

This band is built on the 1293-keV level, which has spin value I=8, as discussed previously. The second level in this sequence, located at 1508 keV, decays to the $I^{\pi}=8^{-}$ metastable state as well as to the 1293-keV bandhead. The 1283-keV transition, which populates the metastable state, displays an angular distribution characteristic of a $\Delta I=1$ dipole transition. This, together with the rather steep slope, displayed by the 215-keV transition in the excitation function data, result in an assignment of I=9 for the 1508-keV level. The remainder of the spins in this band are determined by the appearance of M1/E2 cascade transitions along with stretched E2 crossover transitions. A discussion of the internal structures and configurations of the various states is included in the final chapter.

V. ^{118}Sb EXPERIMENTAL RESULTS

A. Experimental Arrangement

High-spin states in ^{118}Sb were populated using the ^{114}Cd (^{7}Li,3nγ) ^{118}Sb reaction. Two experiments were performed. They were a γ-γ-t coincidence experiment and an excitation function measurement. The ^{7}Li beams were supplied by the Notre Dame tandem Van de Graaff accelerator. The target used was a self-supporting, metallic foil with a thickness of 1 mg cm^{-2}, enriched to about 96% in ^{114}Cd. The measurements were performed with two coaxial Ge(Li) detectors with efficiencies of about 9%. One of the detectors was supplied by Notre Dame. Standard gamma-ray electronics in conjunction with a PDP 9 computer were used for the data acquisition. The data were recorded on magnetic tape and returned to M.S.U. for analysis.

A singles spectrum of ^{118}Sb recorded using this reaction is shown in Figure V-1. This spectrum was taken using a ^{7}Li beam energy of 28 MeV and a detector angle of 125^{o}. As indicated in the figure there are many gamma-rays which result from competing reactions. Several gamma-rays from both of the neighboring Sb isotopes appear in the spectrum. These result from two and four neutron evaporation. In addition, unlike the alpha reaction used to produce ^{116}Sb, with the Li reaction charged particle evaporation makes a non-negligible contribution to the total cross-section. Consequently both ^{115,116}In are populated respectively by α2n and αn evaporation. Gamma-rays associated

Figure V-1 Spectrum of ^{114}Cd (^{7}Li,3nγ) obtained at an angle of 125° with respect to the beam

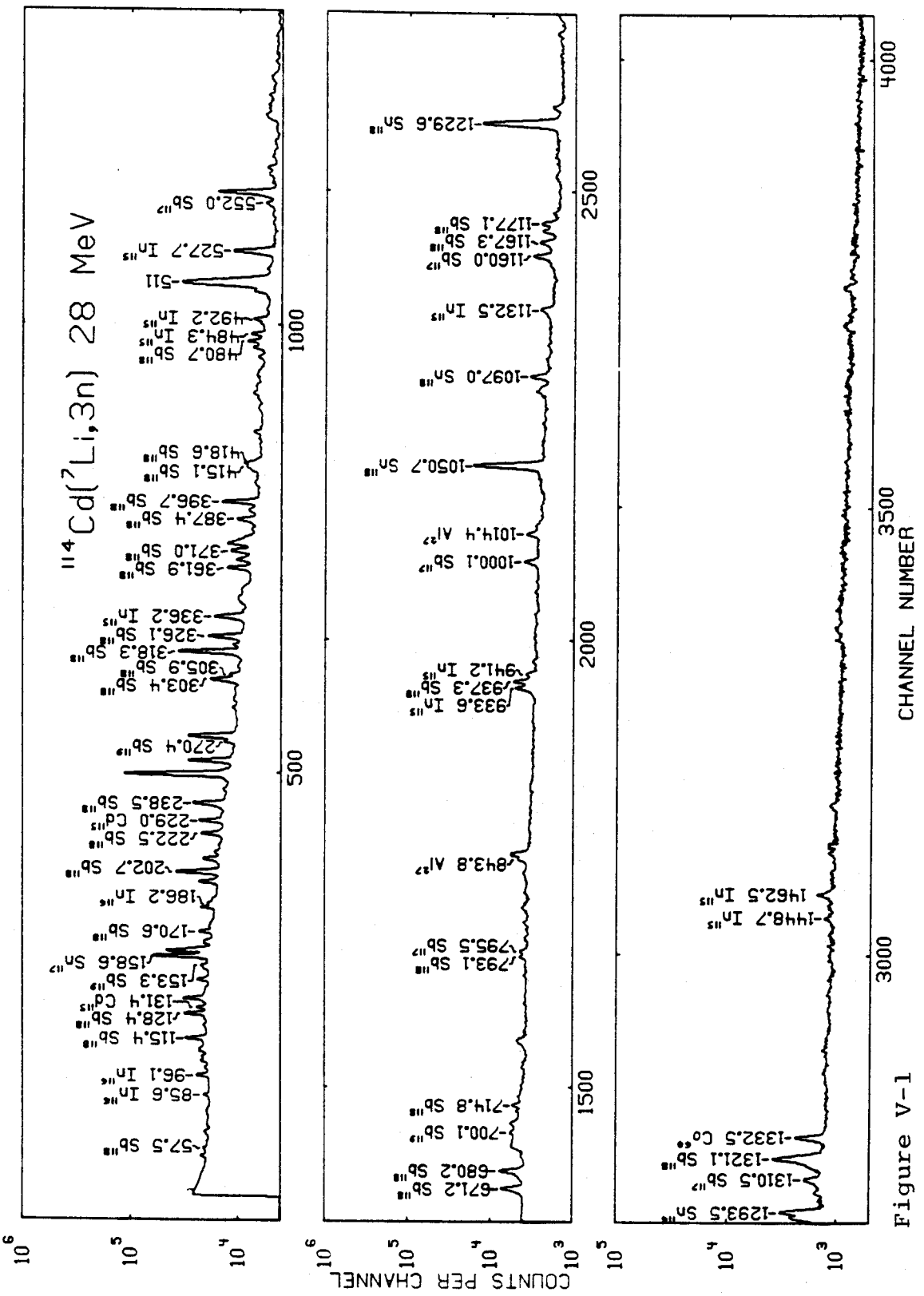
^{114}Cd(^{7}Li,3n) 28 MeV
COUNTS PER CHANNEL
CHANNEL NUMBER
-57.5 Sb^{118}
-85.6 In^{114}
-96.1 In^{114}
-115.4 Sb^{118}
-128.4 Sb^{118}
-131.4 Cd^{115}
-153.3 Sb^{118}
-158.6 Sn^{117}
-170.6 Sb^{118}
-186.2 In^{114}
-202.7 Sb^{118}
-222.5 Sb^{118}
-229.0 Cd^{115}
-238.5 Sb^{118}
-270.4 Sb^{119}
-303.4 Sb^{118}
-305.9 Sb^{118}
-318.3 Sb^{118}
-326.1 Sb^{118}
-336.2 In^{115}
-361.9 Sb^{118}
-371.0 Sb^{118}
-387.4 Sb^{118}
-396.7 Sb^{118}
-415.1 Sb^{118}
-418.6 Sb^{118}
-480.7 Sb^{118}
-484.3 In^{115}
-492.2 In^{115}
-511
-527.7 In^{115}
-552.0 Sb^{117}
-671.2 Sb^{118}
-680.2 Sb^{118}
-700.1 Sb^{117}
-714.8 Sb^{118}
-793.1 Sb^{118}
-795.5 Sb^{117}
-843.8 Al^{27}
-933.6 In^{115}
-937.3 Sb^{118}
-941.2 In^{115}
-1000.1 Sb^{117}
-1014.4 Al^{27}
-1050.7 Sn^{118}
-1097.0 Sn^{118}
-1132.5 In^{115}
-1160.0 Sb^{117}
-1167.3 Sb^{118}
-1177.1 Sb^{118}
-1229.6 Sn^{118}
-1293.5 Sn^{118}
-1310.5 Sb^{117}
-1321.1 Sb^{118}
-1332.5 Co^{56}
-1448.7 In^{115}
1462.5 In^{115}
500
1000
1500
2000
2500
3000
3500
4000

Figure V-1

with ^{115}Cd also appear in the spectrum. This is surprising considering αpn and αd evaporation should have a low cross-section. A possible explanation is that ^{115}Cd was produced by the direct reaction ^{114}Cd (^{7}Li, ^{6}Li) ^{115}Cd. This is supported by the fact that only low-lying, low-spin states were populated, which is not consistent with expectations of a fusion-evaporation reaction at the beam energies used. It is, however, surprising that a direct reaction would have such a large cross-section. It must be that all of these possibilities contribute. In addition to these transitions several Sn gamma-rays appear, which result from the β-decay of the Sb and In nuclei. As with the ^{116}Sb results, no further reference will be made with regards to these transitions except to indicate where they interfere with transitions, resulting from the decay of high-spin levels in ^{116}Sb.

In addition to these experiments using heavy-ion reactions, an angular distribution and a half-life measurement were performed using a ^{120}Sn (p,3nγ) ^{118}Sb reaction. For these experiments 30 MeV proton beams were provided by the M.S.U. cyclotron. The target was a self-supporting metal foil of 0.5 mg cm^{-2} thickness, isotopically enriched to 98% ^{120}Sn. A singles spectrum acquired using this reaction at a detector angle of 125° is shown in Figure V-2.

The gamma-ray energies were determined by simultaneously collecting radiation from the standard long-lived radioactive sources ^{133}Ba and ^{152}Eu. This energy calibration

Figure V-2 Spectrum of ^{120}Sn (p,3nγ) obtained at an angle of 125° with respect to the beam

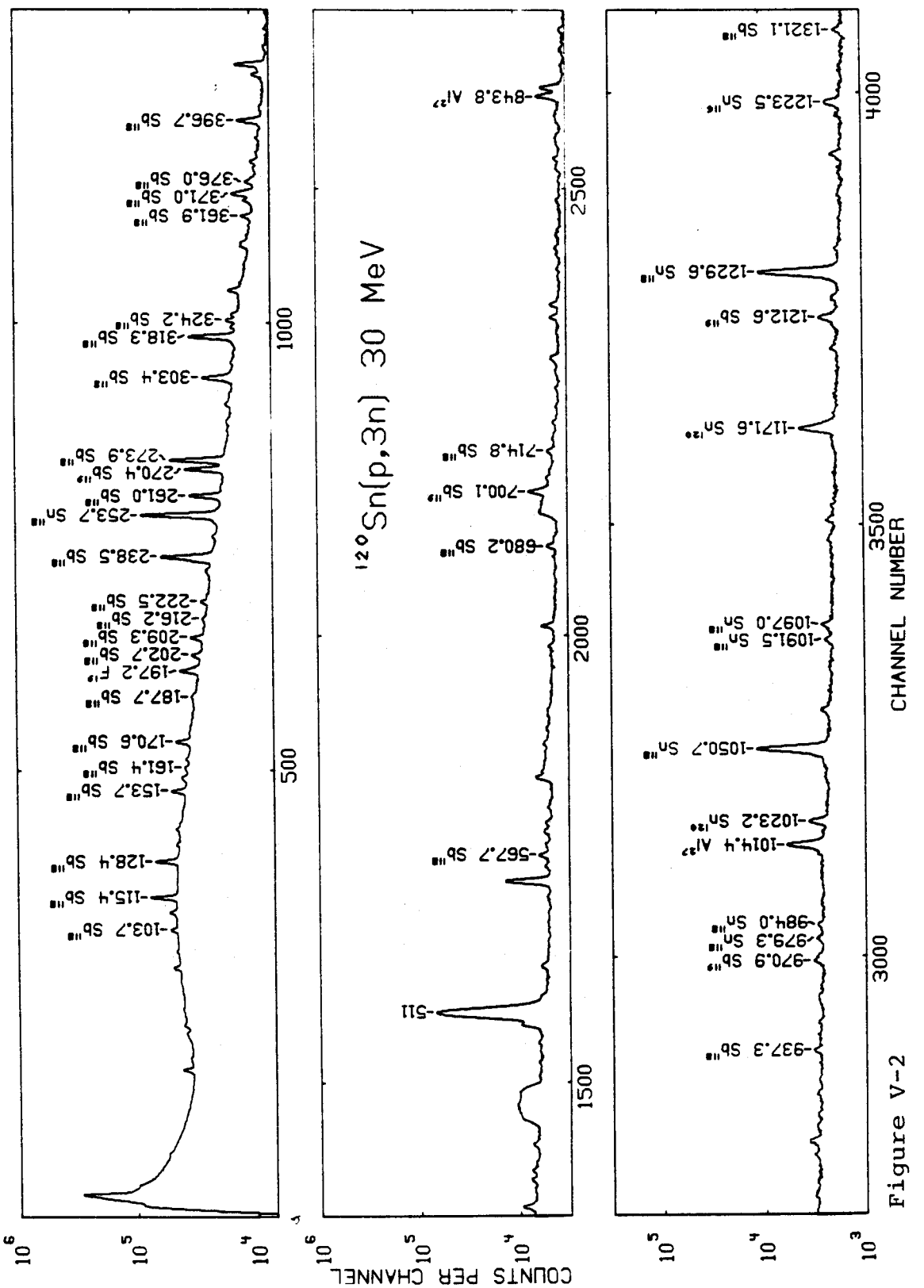
-103.7 Sb118
-115.4 Sb118
-128.4 Sb118
-153.7 Sb118
-161.4 Sb118
-170.6 Sb118
-187.7 Sb118
-197.2 F19
-202.7 Sb118
-209.3 Sb118
-216.2 Sb118
-222.5 Sb118
-238.5 Sb118
-253.7 Sn116
-261.0 Sb118
-270.4 Sb119
-273.9 Sb118
-303.4 Sb118
-318.3 Sb118
-324.2 Sb118
-361.9 Sb118
-371.0 Sb118
-376.0 Sb118
-396.7 Sb118
120Sn(p,3n) 30 MeV
-511
-567.7 Sb118
-680.2 Sb118
-700.1 Sb119
-714.8 Sb118
-843.8 Al27
-937.3 Sb118
-970.9 Sb119
-979.3 Sn118
-984.0 Sn118
-1014.4 Al27
-1023.2 Sn120
-1050.7 Sn118
-1091.5 Sn118
-1097.0 Sn118
-1171.6 Sn120
-1212.6 Sb119
-1229.6 Sn118
-1223.5 Sn116
-1321.1 Sb118
COUNTS PER CHANNEL
CHANNEL NUMBER

Figure V-2

was corroborated by the many gamma-rays of known energy appearing in the spectrum.

B. Results of γ-γ-t Coincidence Experiment

The coincidence experiment was performed using a 26 MeV ^{7}Li beam. Two coaxial Ge(Li) detectors were placed at $+90^{o}$ and -125^{o} with respect to the beam direction. Approximately $2x10^{7}$ coincidence events were collected. Figure V-3 shows several examples of the gated spectra. The results of this experiment are given in Table V-1.

C. Results of Excitation Function Measurement

For this experiment ^{7}Li beams of 22, 24, 26, 28 and 30 MeV were used. A coaxial Ge(Li) detector was positioned at 125^{o} with respect to the beam direction and recorded singles spectra for approximately two hours at each energy. Table V-2 includes the relative intensities determined from the 28 MeV run. They are corrected for detector efficiency and normalized such that the 318 keV transition has the value 100. Figure V-4 shows plots of the intensity as a function of energy obtained from this experiment for some of the more intense transitions.

D. Results of the Angular Distribution Experiment

Two angular distribution experiments were performed for ^{118}Sb. The first involved the use of a high resolution (.7 kev at 122 keV) small volume planar Ge(Li) detector. This made possible the partial resolution of several low energy multiplets. However, because the efficiency of this detector drops off sharply above about 200 keV, no

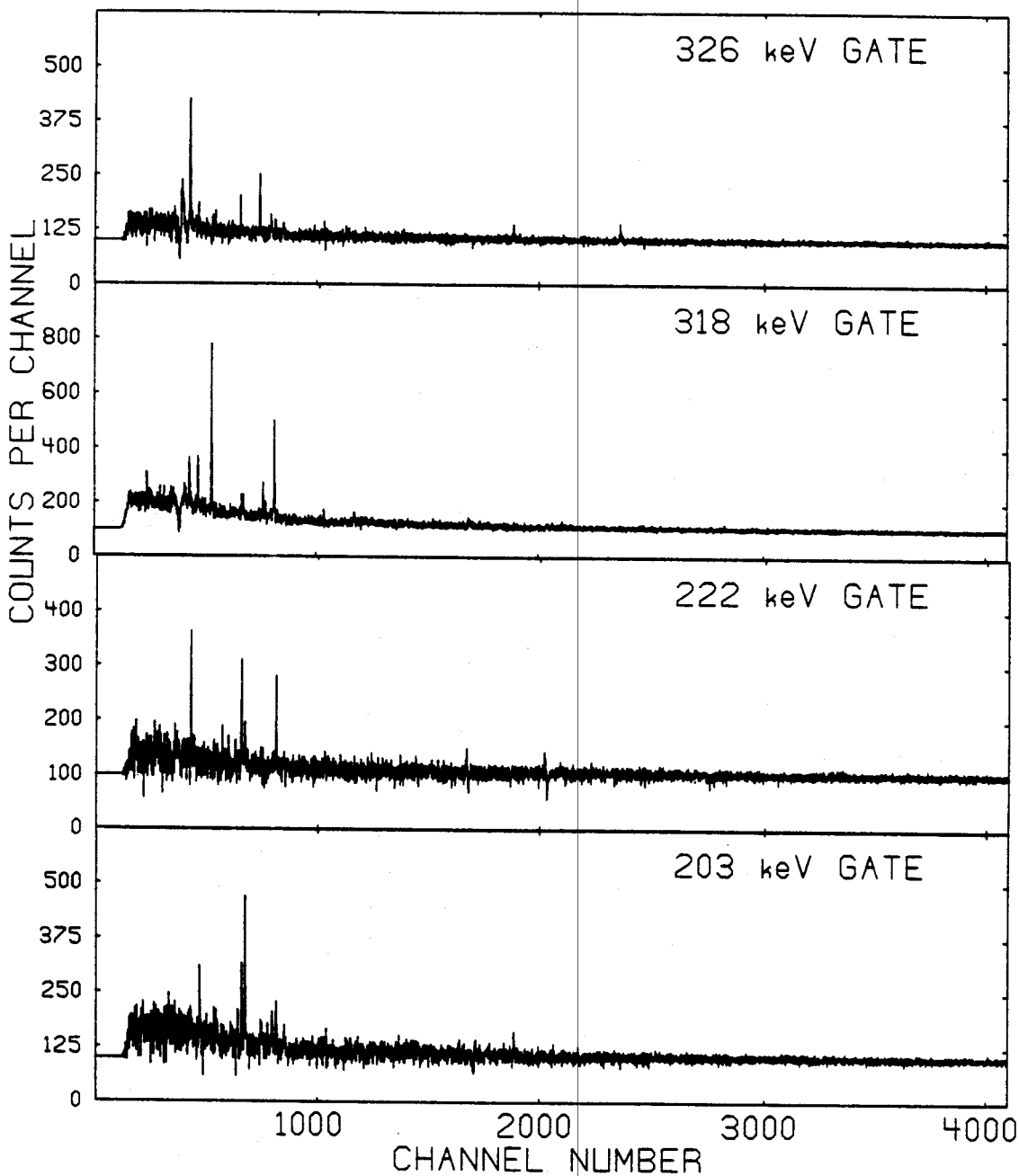

Figure V-3 Results of γ-γ-t coincidence experiment for transitions in ^{118}Sb

Table V-1. Results of γ-γ-t coincidence experiment for transitions in ^{118}Sb.

Gate Energy (keV)	Coincident Gamma-rays (keV)
109	253, 318
152	1321
161	368(a), 378, 481, 490, 600(a), (641), 671, 1321
203(b,c)	96(b,a), 153(c,a), 223, (237)(c,a), 261, 297, 318, 326, 362, 387, 397, 415, 465(a), 507(c,a), (619), (677), (715), 937
223	203, 318, 326, 362, 397, 715, (749)(a)
253(d)	109, 318, 1051(d,a), (1092)(d,a), 1230(d,a)
261(e)	203, 231(e,a), 326, 345(e,a), (362), 415, 490(a), 677, 690(e,a)
297	(203)
306	1167
318	109, 203, 223, 253, 322, 326, 362, 371, 376, 387, 393, 397, (404)(a), 580(a), 619, (836)(a), (1014)(a)
322	(203), 297, 318
326	203, 223, 297, 318, 362, 387, 397, (415), 937, 1177
362(f)	135(f,a), 203, 223, 270(f,a), 318, 326, 335(f,a), 370(f,a), 382(f,a), 387, 397, (415), 700(f,a), (937)
371(f)	135(f,a), 270(f,a), 318, 335(f,a), 362(f,a), 376, 382(f,a), 393, 397, (419), (444)(a), (660)(a), 700(f,a), 715, 769
376(c,g)	115(c,a), 254(a), 261, 318, 337(g,a), 366(g,a), 371, (393), 397, (419) (907)(a), 1160(g,c)
378	161, 671, 1321

Table V-1 continued

Gate Energy (keV)	Coincident Gamma-rays (keV)
387	203, (223), 253(a), 270(a), 326, 362, 397, 415
393	318, 371, 376, 397, (404)(a), 419, (715), (907)(a)
397	203, 223, (254)(a), 261, 318, 326, (362), 371, 376, 393, 419, 747
415(c,h)	203, 209(c,a), 273(c,a), 304(c,a), 326, 362, (387), 795(a), 819(h,a), 1294(h,a)
481	161, (190)(a), 671, (1321)
490	(161), 190(a), (481), (671), 842(a), (1321)
619	318
671	(152), 161, (242)(a), 378, (391)(a), 481, (490), 1321
677	261
680	793, 941(a)
793	680
937(i)	183(a,i), 203, 326
1167	306
1177	326, 362
1321	152, 161, (378), (481), 671

a) These transitions have not been placed in the level scheme.
b) A transition with this energy is known to occur in ^{116}In.
c) A transition with this energy is known to occur in the low spin level scheme of ^{118}Sb.
d) as (b) but ^{118}Sn
e) as (b) but ^{115}In
f) as (b) but ^{119}Sb
g) as (b) but ^{117}Sb
h) as (b) but ^{116}Sn
i) as (b) but ^{18}F

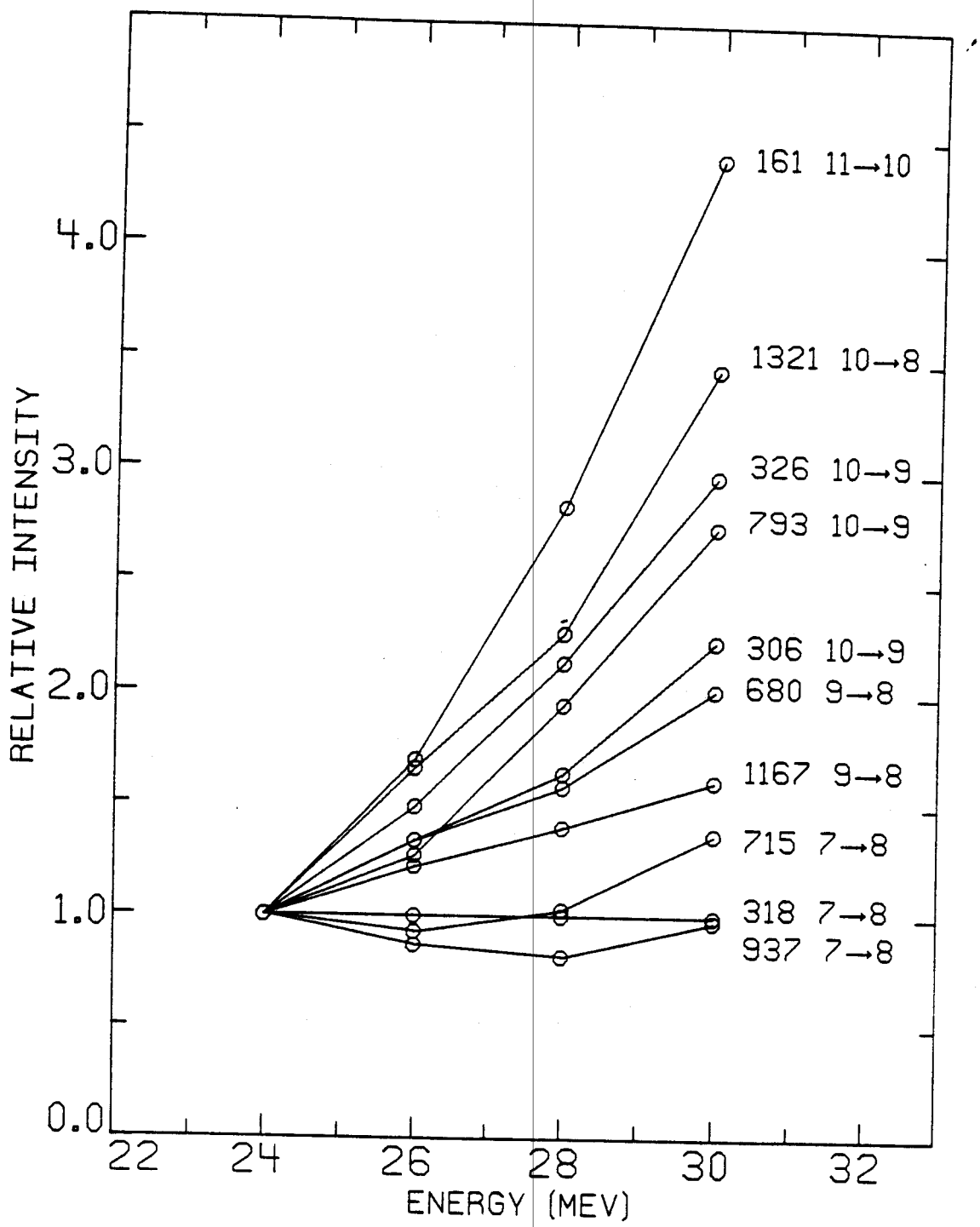

Figure V-4 Excitation functions for transitions in ^{118}Sb

information on higher lying transitions could be obtained.

A second experiment using a coaxial Ge(Li) detector of about 9% efficiency was performed to obtain angular distributions for the higher energy transitions. Normalization between angles is achieved in the first experiment by using x-rays. These are emitted isotropically and have sufficiently high energy to be detected by the low energy planar detector. In the second experiment a second Ge(Li) detector was positioned at a fixed angle of -135° with respect to the beam. Data were collected at each angle for about two hours.

Table V-2 shows the angular distribution coefficients determined in these experiments. For energies less than 300 keV the values are taken from the first experiment. Results for energies above that are taken from the second experiment. Examples of the angular distributions are plotted in Figure V-5.

E. Results of Half-life Experiment

For this experiment the high resolution planar Ge(Li) detector was positioned at 90° with respect to the beam direction. Data were collected into 10 separate time spectra each corresponding to a period of 7.65±0.05 nsec. Half-lives were obtained for two delayed transitions associated with the decay of the 927 keV level. A half-life of 21.7±1.4 nsec. is assigned to this level. A plot of intensity as a function of time for these transitions is shown in Figure V-6.

Table V-2 Energies (E_γ), relative intensities (I_o), angular distribution coefficients, and spin assignments for transitions in ^{118}Sb.

E_γ (a) (keV)	I_o (b) rel.	A_2/A_0	A_4/A_0	$I_i \rightarrow I_f$
37.1 (e)				(8)→7
57.5	13.7			
108.8	8.7	-0.25±0.09	-0.05±0.14	
152.1 (d)	5.4	0.62±0.20		(10)→10
161.4	57.4	-0.29±0.07	0.01±0.10	11→10
202.7 (c)	44.0			9→(8)
222.5	17.7	0.37±0.03	-0.05±0.04	7→7
253.2 (c)	31.7			
261.0	40.3	0.11±0.02	0.01±0.03	
297.4 (d)	2.4	-0.26±0.12		7→(8)
305.9 (c)	10.2			(10)→9
318.3	100.0	-0.09±0.01	-0.06±0.04	7→8
321.6	9.5	-0.18±0.04	-0.05±0.05	(8)→7

Table V-2 continued

E_γ(a) (keV)	I_o(b) rel.	A_2/A_0	A_4/A_0	$I_i \rightarrow I_f$
326.1	44.3	-0.02±0.05	-0.03±0.07	10→9
361.9	24.8	-0.03±0.03	0.00±0.04	11→10
371.0	18.5	0.30±0.03	-0.01±0.04	8→7
376.0	15.3	0.20±0.06	-0.12±0.09	9→8
377.8	8.8			
387.4(c)	19.6			(12)→11
392.6(d)	5.2	0.22±0.17		10→9
396.7	38.3	0.11±0.01	-0.06±0.01	7→7
415.1(c)	13.1			13→12
418.6(c)	3.1			(11)→10
480.7(c)	19.1			
489.9(c)	6.2			
619.0(c)	6.3			7→7

Table V-2 continued

E_γ(a) (keV)	I_o(b) rel.	A_2/A_0	A_4/A_0	$I_i \rightarrow I_f$
640.8	2.5			10→9
671.2(c)	40.5			
676.5(c)	6.9			
680.2	46.9	-0.60±.02	0.01±0.02	9→8
714.8	15.4	-0.09±0.02	-0.04±0.04	7→8
746.9(c)				9→7
768.5(c)	2.0			10→8
793.1	11.8			(10)→9
937.3	44.8	-0.24±0.05	-0.02±0.08	7→8
1167.3	29.4	-0.99±0.07	0.12±0.10	9→8
1177.1(d)	28.3	-0.67±0.19		9→8
1321.1	75.4	0.17±0.04	-0.21±0.07	10→8

a) Energy uncertainties are 0.2 keV for most transitions, rising to 0.5 keV for weak transitions and components of multiplets.
b) Intensity uncertainties are approximately 15% for most transitions, rising to 30% for weak transitions and components of multiplets.

Table V-2 continued

c) These are transitions which are too weak to fit or are components of unresolvable multiplets.
d) These are weak transitions for which A_4 was set to zero during the fitting procedure.
e) This transition was not observed. Its energy was determined from level energy differences.

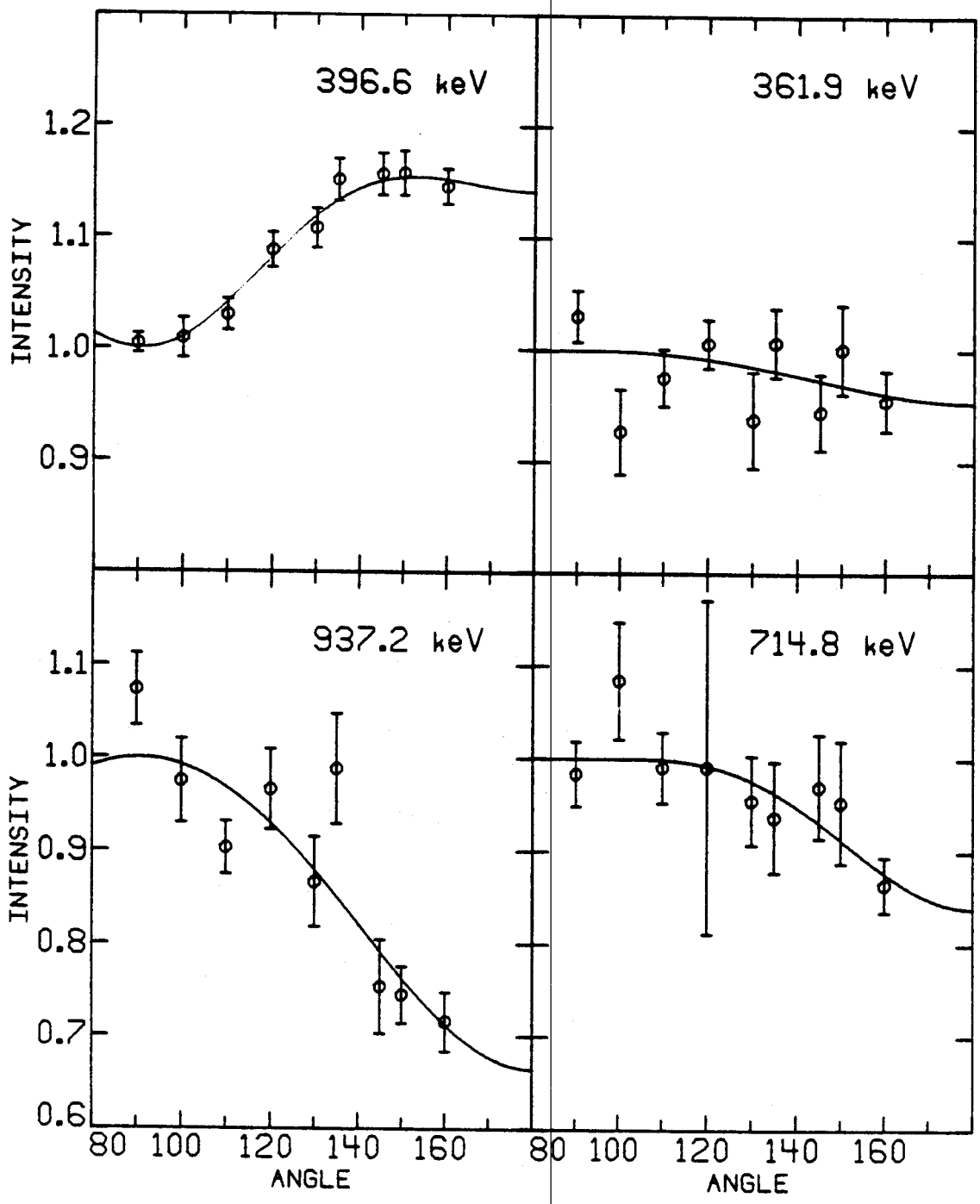

Figure V-5 Angular distributions for selected ^{118}Sb transitions. The fits are normalized to 1 at 90°

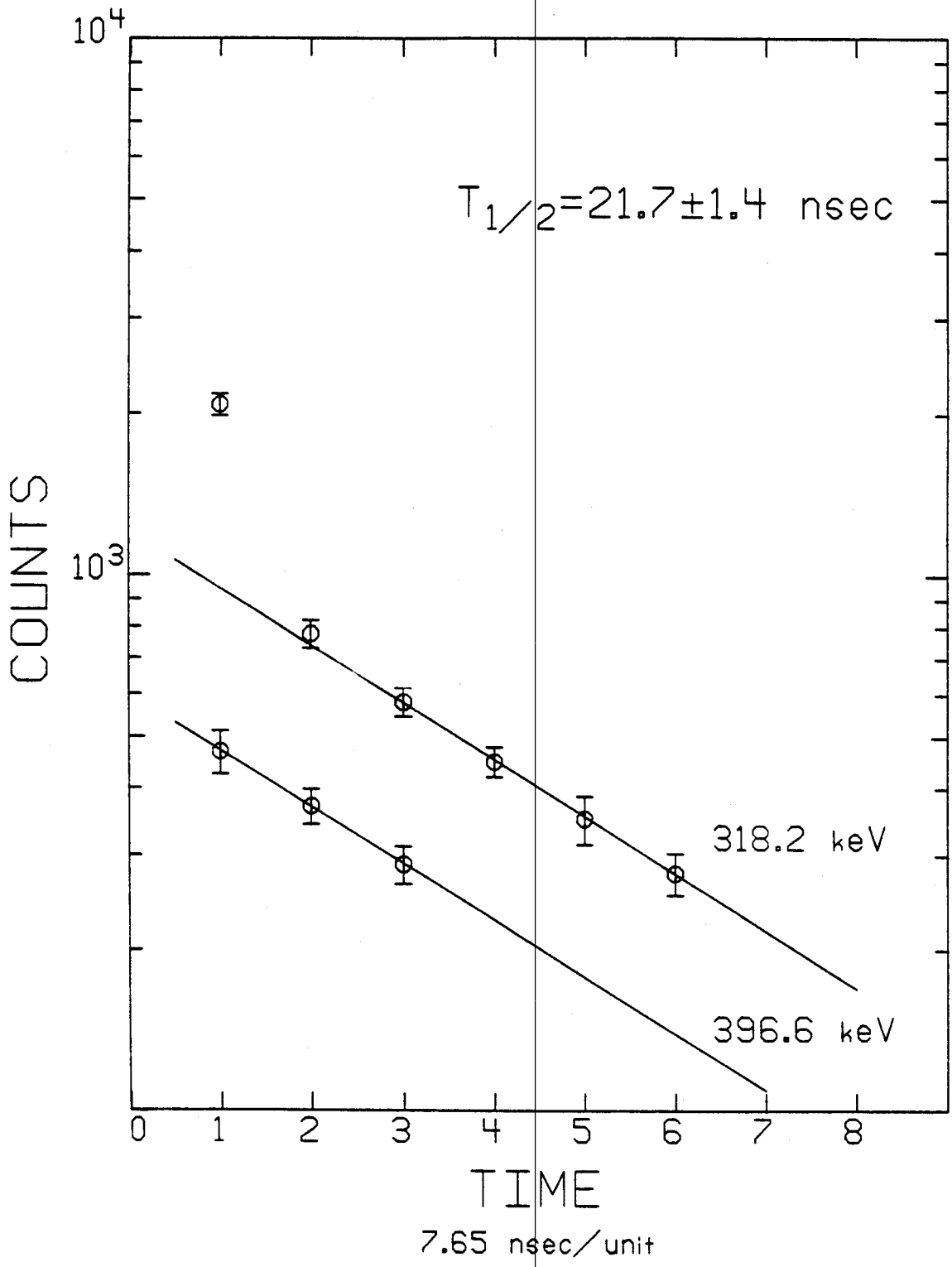

Figure V-6 Half-life data for transitions occurring in the decay of the isomer at 927 keV

F. ^{118}Sb Level Scheme

The ^{118}Sb level scheme was constructed in the same manner as described for ^{116}Sb. It is depicted in Figure V-7. This level scheme contains 38 transitions depopulating 26 levels. Except for the lowest lying level in the scheme with energy 212 keV, all of the transitions and levels have not been previously studied. Although as can be seen from Table V-2 several of the transitions are parts of multiplets, they can be placed unambiguously in the level scheme.

The only difficulty involved in the placement of transitions in this level scheme occurs for the 37 keV transition. This transition was not observed in any of the experiments. Its existence is required by the placement of the 1177 keV transition which depopulates the 1389 keV level, along with coincidence relationships, which require there be a sequence of gamma-rays which connect the 1389 and 1149 keV levels. This requires that the 203 and 37 keV transitions be in cascade with each other, while connecting the 1389 and 1149 keV levels. The order of the two transitions, however, cannot be determined unambiguously. It was chosen in the manner displayed in the level scheme to be consistent with the results for ^{116}Sb. Although this selection is not experimentally rigorous, the extreme similarity between the two nuclei with respect to this I=8 band (maximum energy difference between corresponding band members in the two nuclei is 10 keV or about 3%) indicates the 203 keV transitions should be placed as the lowest band member.

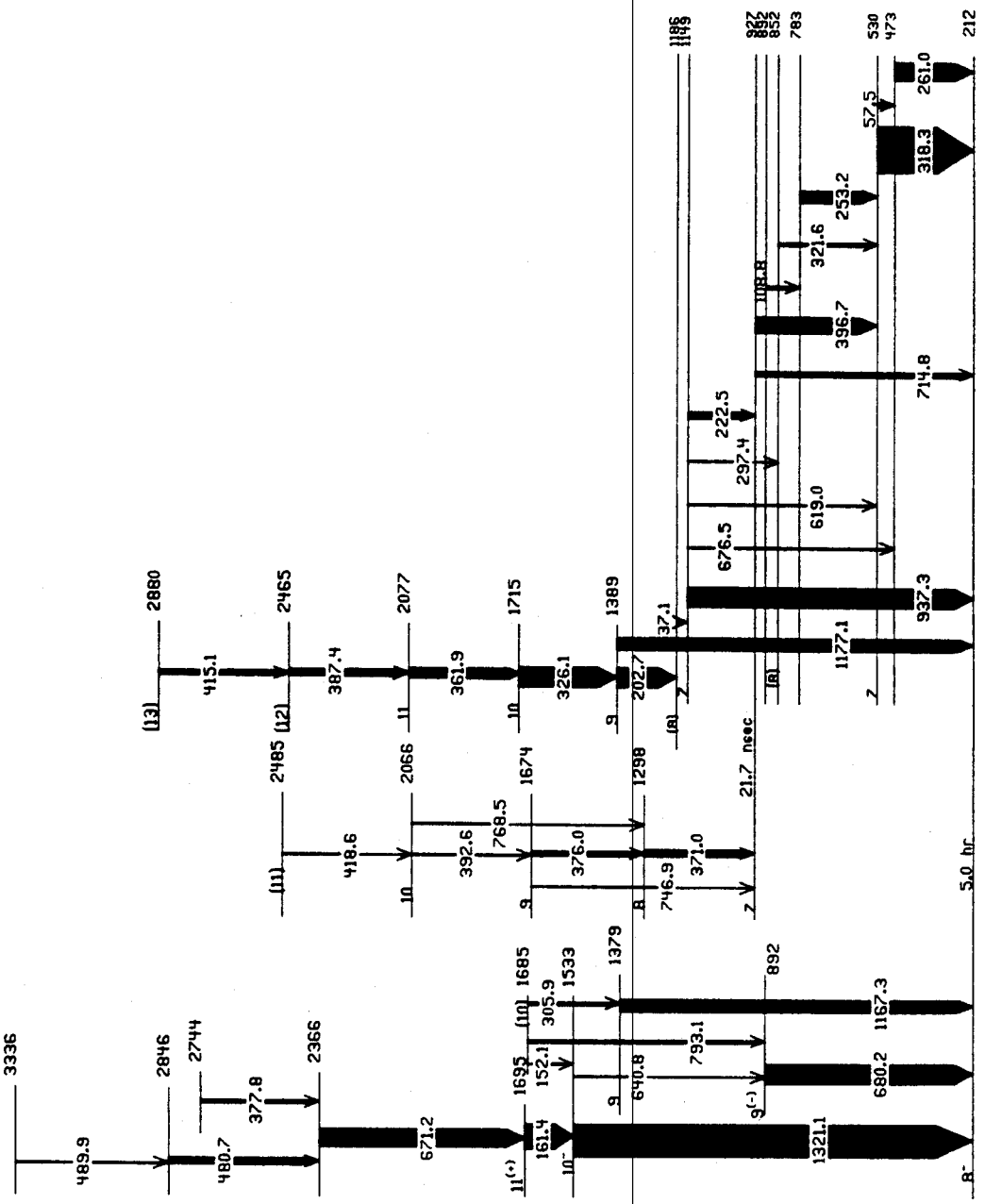

Figure V-7 High-spin level scheme for ^{118}Sb

This argument is also true in general for the two nuclei. A comparison of the two level schemes for ^{116,118}Sb reveals a striking amount of similarity in the high-spin structure of these nuclei. This can be seen in the transitions energies, intensities and angular distribution coefficients. This is not unexpected, as there is only a difference of two paired neutrons in the internal composition of these two nuclei. Since the level structure is determined predominantly by the unpaired odd particles, the extremely similar level structure is merely the result of having the same single particle orbitals available for the odd particles to occupy. Because of this similarity in the results for the most intense transitions, a systematic correspondence is established between many of the levels. These systematics lend support to the correctness of each level scheme individually as well as provide supporting evidence for the assignment of spins and parities based on these systematics. This is especially helpful for ^{118}Sb.

G. Spin and Parity Assignments

1. The 8^- Metastable State

As in ^{118}Sb the lowest level in the scheme can be established to be the $I^{\pi}=8^-$, 5.0 hr. metastable state of ^{116}Sb. The spin was determined using the atomic-beam magnetic resonance method.[30] The level energy was determined to be 212±8 keV from beta-decay studies.[33] These values have been adopted here.

For convenience of discussion the transitions and levels will be divided into four groups. The first of

these is the sequence of gamma-rays which depopulate through the 680, 1167, and 1321 keV transitions. These are displayed on the left in Figure V-7. They will be referred to as the high spin sequence. The second group includes those remaining transitions which depopulate levels lying below 1200 keV. These are drawn on the right in Figure V-7. They will be referred to as the medium spin levels. The last two groups will be the bands built on the I=7 state at 927 keV and the band built on the I=(8) state at 1186 keV.

2. High Spin Sequence

The first level in this sequence is at 892 keV and is depopulated by the 680 keV transition. This transition displays a negative A_2 angular distribution coefficient, indicative of a $\Delta I=1$ transition. The excitation function results for this transition display a rather steep slope, indicating high spin. Therefore an assignment of $I^{\pi}=9^{(-)}$ is made for this level. The parity is tentatively assigned as being negative on the basis of systematics with ^{116}Sb.

The second level in this sequence is at 1379. This level is assigned to have I=9. This assignment is determined by the $\Delta I=1$ behavior of the angular distribution of the 1167 keV transition, along with its high spin excitation function behavior.

The next level in this sequence is at 1533 keV and is depopulated by the 1321 keV transition. This transition displays a positive A_2 and a negative A_4 angular distribution coefficients, indicative of an E2 transition. This results in an assignment of $I^{\pi}=10^{-}$ to this level.

The next level is at 1685 keV. It is tentatively assigned to have I=(10) on the basis of the excitation function data of the 306 keV level.

The next level in this sequence is at 1695 keV and is depopulated by the 161 keV transition. This level is assigned to have $I^{\pi}=11^{(+)}$. The spin is determined by the $\Delta I=1$ behavior of the angular distribution of the 161 keV transition. The parity is tentatively assigned on the basis of systematics with ^{116}Sb.

No assignments are made for higher lying levels in this sequence. This is because these levels were not populated in the angular distribution experiment using the $(p,3n\gamma)$ reaction. This fact, however, indicates they are high spin states, which is again consistent with the results from ^{116}Sb.

3. Medium Spin States

The three transitions of energies 937, 715, and 318 all decay to the 8^- metastable state. In addition they all display negative A_2 coefficients in their angular distributions, indicating they are $\Delta I=1$ transitions. This results in an I=7 or 9 assignment for the levels at 530, 927, and 1149 keV. The excitation functions for transitions depopulating these levels indicate that the smaller of these two values is the correct alternative in all three cases. This is also consistent with the results for corresponding levels in ^{116}Sb. Therefore spin assignments of I=7 are made for the 530, 927, and 1149 keV levels. It should be noted

that these assignments are consistent with the angular distribution results of the interconnecting transitions with energies 222 and 397 keV.

The 852 keV level is tentatively assigned to have I=(8). This assignment is made on the basis of the $\Delta I=1$ character of the angular distribution for the 322 keV transition, which depopulates this level. There is insufficient information available to make further spin assignments for levels in this group.

4. The I=7 Band

This band is built on the 927 keV level, with spin value I=7 as discussed above. Angular distributions for three of the transitions in this band were obtained. These are the 371, 376, and 392 keV transitions. The angular distributions are consistent with M1/E2 multipolarities with substantial positive mixing ratios ($\delta \simeq 0.3$). The cross-over transitions are too weak to obtain any angular distribution information. Spin values are assigned to this band consistent with a $\Delta I=1$ increasing spin sequence. The tentative spin assignment of I=(11) for the highest member of this band is made on the basis of these systematics.

5. The I=8 Band

The second band member located at 1389 keV depopulates by means of the 1177 keV transition to the 8^- metastable state. The angular distribution for this transition displays characteristic $\Delta I=1$ behavior, thus requiring the 1389 keV level to have a spin of I=7 or 9. The excitation

function for this transiton indicates the higher spin value is the correct alternative. This is again consistent with results from ^{116}Sb. Consequently an assignment of I=9 is given to this level.

Angular distributions were obtained for the 203, 326, and 362 keV transitions. Although it should be noted the 203 and 362 keV lines are known to contain contributions from other gamma-rays. The angular distribution coefficients are consistent with $\Delta I=1$, M1/E2 transitions. The mixing ratio ($\delta \simeq 0.1$) for these transitions is smaller than those obtained for the I=7 band. Tentative spin assignments are made for this band consistent with a $\Delta I=1$ increasing spin sequence. A discussion of these structures is included in the next chapter.

VI. DISCUSSION AND SUMMARY

A. High-Spin Sequence

The high-spin structure of odd-odd Sb nuclei is very closely related to that of the neighboring odd mass Sb nuclei. This is mainly due to the dominance of the high-spin $1h_{11/2}$ unique-parity single-particle orbital which is readily available for occupancy by the additional odd neutron in these nuclei. Excitation of the $1h_{11/2}$ orbital requires only a few hundred keV of energy and provides at least two additional units of available angular momentum over any other easily accessible neutron single-particle state. Consequenly it would be expected that the structure of the yrast levels in ^{116,118}Sb should result from a coupling of the yrast levels in the neighboring odd mass Sb nuclei to the high spin $1h_{11/2}$ neutron state.

Figure VI-1 shows the high-spin sequence for $^{115\text{-}119}$Sb. Also indicated in the figure are some pertinent yrast states from the even Sn cores. The odd-odd Sb nuclei are normalized to the $I^{\pi}=8^{-}$ metastable states, while the odd mass Sb nuclei are shown beginning from their $I^{\pi}=5^{+}/2$ ground states. The similarity of the level energies and spacings is immediately apparent from the figure. Qualitatively the situation may be described as a systematic series of states. The first of which begins in ^{115}Sb at 724 keV and steadily decreases in energy to 270 keV in ^{119}Sb. This is followed by a series of two states at about 1300 keV that remain fairly constant over the mass range shown. This is followed by a large gap

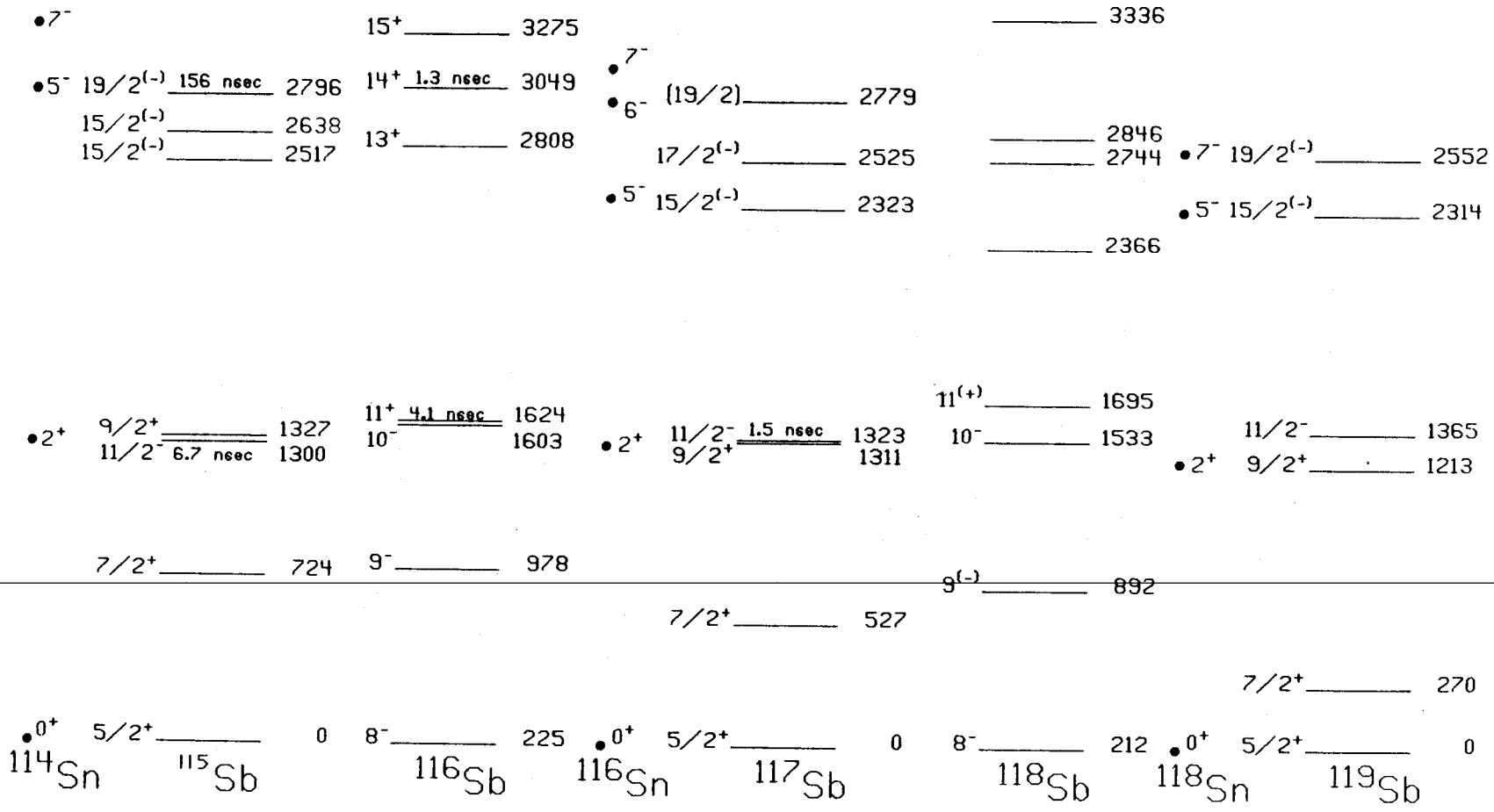

Figure VI-1 High-spin sequence of levels in ^{116,118}Sb compared with similar levels from odd mass Sb nuclei and doubly even Sn core nuclei

in energy and then several closely spaced high lying states. Each of these states will now be considered in more detail.

The structure of the $I^{\pi}=8^{-}$ states in the odd-odd nuclei is thought to consist predominantly of the $2d_{5/2}$ proton coupled to maximum spin with the $1h_{11/2}$ neutron single-particle states.[34] This assignment agrees rather well with the systematics established here. The $2d_{5/2}$ proton state is the lowest lying single-particle proton state for these nuclei and it is this state which is responsible for the $I^{\pi}=5^{+}/2$ odd mass ground states. Other available proton single-particle states are the $1g_{7/2}$ and $1h_{11/2}$. These appear as the $I^{\pi}=7^{+}/2$ and $11^{-}/2$ states in the odd mass Sb nuclei. Coupling these to maximum spin with a $1h_{11/2}$ neutron results in $I^{\pi}=9^{-}$ and 11^{+} states. From the figure it is evident that these configurations correspond to the experimentally observed yrast levels of the same spin in $^{116,118}Sb$.

The $I^{\pi}=10^{-}$ states located at 1602 and 1512 keV respectively in ^{116}Sb and ^{118}Sb, lie 1377 and 1322 keV above their respective $I^{\pi}=8^{-}$ metastable states. These energies are approximately the same as the first $I^{\pi}=2^{+}$ phonon excitation in the even Sn cores. Consequently these states might be characterized as being predominantly a $2d_{5/2}$ proton and $1h_{11/2}$ neutron single-particle states coupled to the first quadrupole phonon core excitation. This is consistent with the systematics established by the neighboring odd mass Sb nuclei and the configuration assignments made for the corresponding $I^{\pi}=9^{+}/2$ levels in these nuclei.

The higher lying levels in these sequences are most likely four quasiparticle states made from three-neutron, one-proton configurations. This is plausible because the high-spin states in the Sn core nuclei have been found to be relatively pure two-neutron states.[35] For example there is a $I^{\pi}=5^{-}$ state at 2815 keV in ^{114}Sn. This state coupled to maximum spin with a $2d_{5/2}$ proton is the proposed[7] configuration for the 2517 keV, $I^{\pi}=15^{-}/2$ level in ^{115}Sb. Coupling this state to maximum spin with another $1h_{11/2}$ neutron will result in a $I^{\pi}=13^{+}$ level in ^{116}Sb. This is most likely the configuration for the observed $I^{\pi}=13^{+}$ level at 2808 keV. This configuration may also be consistent for the 2366 keV level in ^{118}Sb. The decrease in energy with respect to this level in ^{116}Sb may be part of a systematic trend because the $I^{\pi}=5^{-}$ level in ^{116}Sn is about 500 keV lower than the same state in ^{114}Sn. Similarly, the $I^{\pi}=15^{+}$ level in ^{116}Sb may result from the $I^{\pi}=7^{-}$ core excitation in ^{114}Sn. Due to the lack of definite experimental spin information for higher lying levels, especially in ^{118}Sb, a discussion of possible configurations is unjustified. However, in general these levels can be described as two neutron core excitation states coupled to the odd proton in either the $2d_{5/2}$ or $1g_{7/2}$ state and the odd neutron in the $1h_{11/2}$ state.

B. Medium Spin Levels

Those levels which lie below 1200 keV and are not members of the two band structures can be characterized as having spin values between I=6 and I=9. In addition since the first

phonon excitation requires more than 1300 keV and the first two-particle Sn core excitations require more than 2 MeV, these states must be described in terms of two coupled single-particle excitations. These states are primarily then alternative couplings of the same two-particle states that made up the lower levels of the yrast sequence. The $1h_{11/2}$ neutron can be coupled to the $2d_{5/2}$, $1g_{7/2}$ and $1h_{11/2}$ proton levels resulting in several possible high-spin states. Additional configurations that may contribute states to this energy region are the $\{(\pi h_{11/2})\ (\nu d_{3/2})\}$ and $\{(\pi g_{7/2})\ (\nu g_{7/2})^{-1}\}$. A final possibility for forming high-spin states at about this energy involves the $g_{9/2}$ proton hole state. It is this state which is principally responsible for the band structure that is observed. However, it is not possible to rule out this orbital as also contributing to levels which are not directly associated with the band structures. It is possible to make estimates of where each of these configurations should lie based upon single-particle energies determined from states in the neighboring nuclei. However, because of the large number of possible states and the complexity of the states, detailed shell model calculations including the effects of the p-n residual interaction would be necessary before specific configuration assignments could be made.

C. Deformed States

In each of the nuclei under study two bands, one built on a spin I=7 state the other built on a spin I=8 state,

were observed. These bands exhibit very characteristic rotational behavior, in that they are composed of I→I-1 mixed M1/E2 transitions, while additionally in some cases displaying E2 crossover transitions. The energy spacings between band members are also consistent with a rotational interpretation. Consequently they will be discussed here in those terms.

As with the other states in this region because of energy considerations the bandheads must be predominantly two-particle states. In considering the structure of these states it is once again helpful to look at the neighboring odd mass Sb nuclei. The existence of bands built on a $g_{9/2}$ proton hole state in those nuclei leads to the reasonable assumption that the bands in the odd-odd nuclei also involve a proton in this orbital. A few observations support this assumption. First the excitation energies of the bandheads in the odd-odd case are very similar to the excitation energy of the $I^{\pi}=9^{+}/2$ bandhead in the neighboring odd mass nuclei. In addition the high spin nature of the bandheads would require a large angular momentum contribution from the proton single-particle orbital. Figure VI-2 shows the Nilsson levels for the odd proton. It is clearly evident that the only easily accessible high-spin orbital is the $9^{+}/2\{404\}$, which is derived from the $g_{9/2}$ shell model orbital. Finally this assignment is consistent with total potential energy calculations[12] which show the $9^{+}/2\{404\}$ Nilsson level displaying a minimum at a non-zero deformation for Z=51

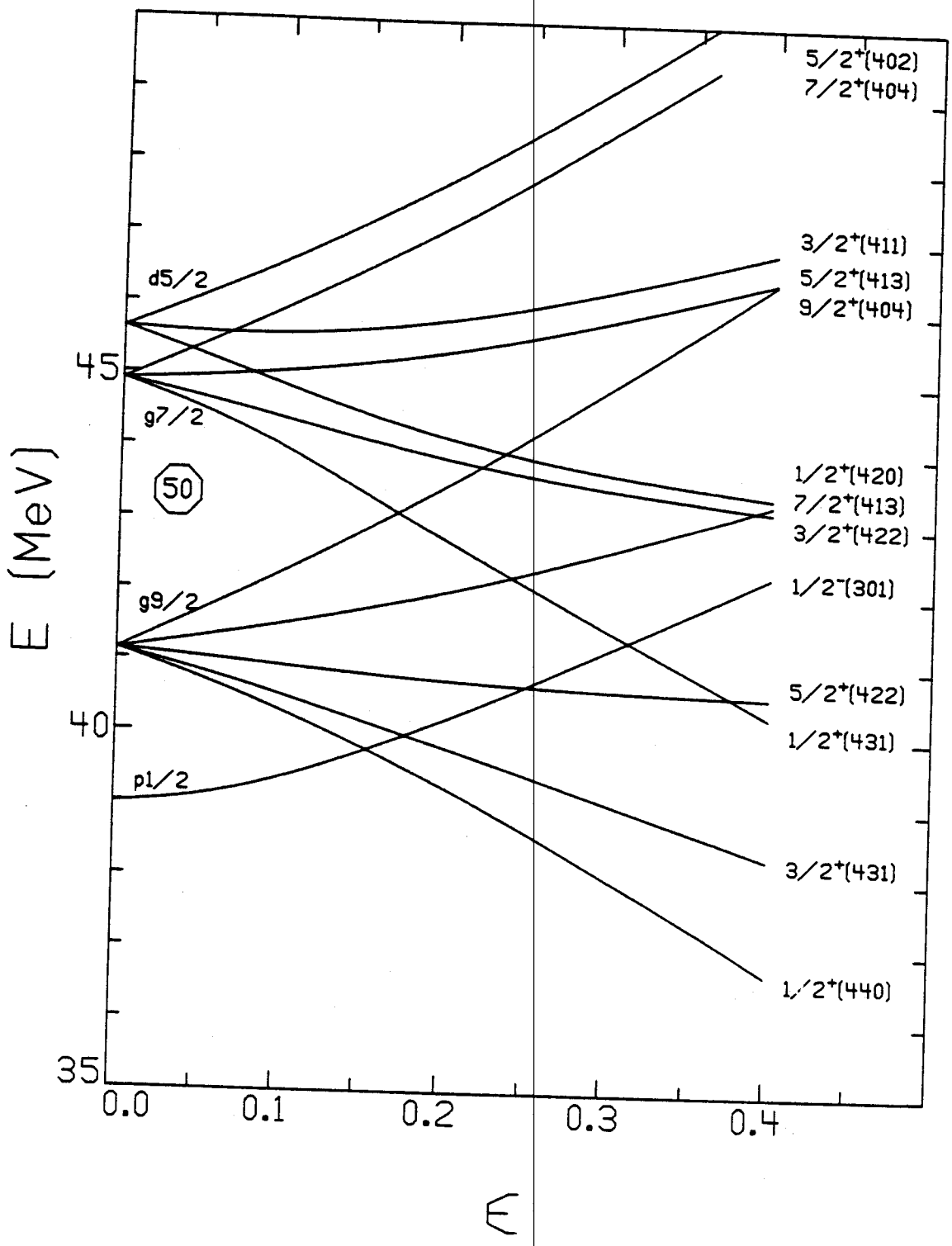

Figure VI-2 Nilsson diagram for odd protons

nuclei. For the higher lying J=8, there is one additional argument that can be made, which involves the band energy spacing. This will be discussed later.

The Nilsson levels for the odd neutron are shown in Figure VI-3. Available high-spin orbitals for the neutron to occupy include the $1h_{11/2}$ and $1g_{7/2}$ shell model orbitals. Assuming a model in which the particles are strongly coupled to the deformed core, K the projection of the total angular momentum on the deformation axis is a good quantum number. It is given by $K = |K_1 \pm K_2|$ where K_i is the projection of the angular momentum of the i^{th} particle on this same axis. Taking the proton to be in the $K_1^{\pi}=9^+/2$ {404} Nilsson orbital and assuming a neutron Fermi energy of about 51 MeV, it is evident from Figure VI-3 that in order to form a K=8 rotational band the neutron must be in the $7^+/2$ {404} Nilsson orbital. Similarly for the K=7 band, the neutron must be in either the $5^+/2${404} or the $5^-/2${532} orbitals. This strong coupling description of the K=8 band will not be considered.

A plot of $(E_I - E_{I-1})/2I$ as a function of $2I^2$ for the two bands is shown in Figure VI-4. In a plot such as this the intercept is the rotational constant $\frac{\hbar^2}{2\theta}$, and perturbation effects on the simple rotor model are emphasized. A rotational band which has only the I(I+1) energy dependence would appear on this type of plot as a horizontal line. It is immediately obvious that the K=8 bands, except for the first level, display this horizontal behavior to a remarkable degree of accuracy. This is extremely compelling evidence

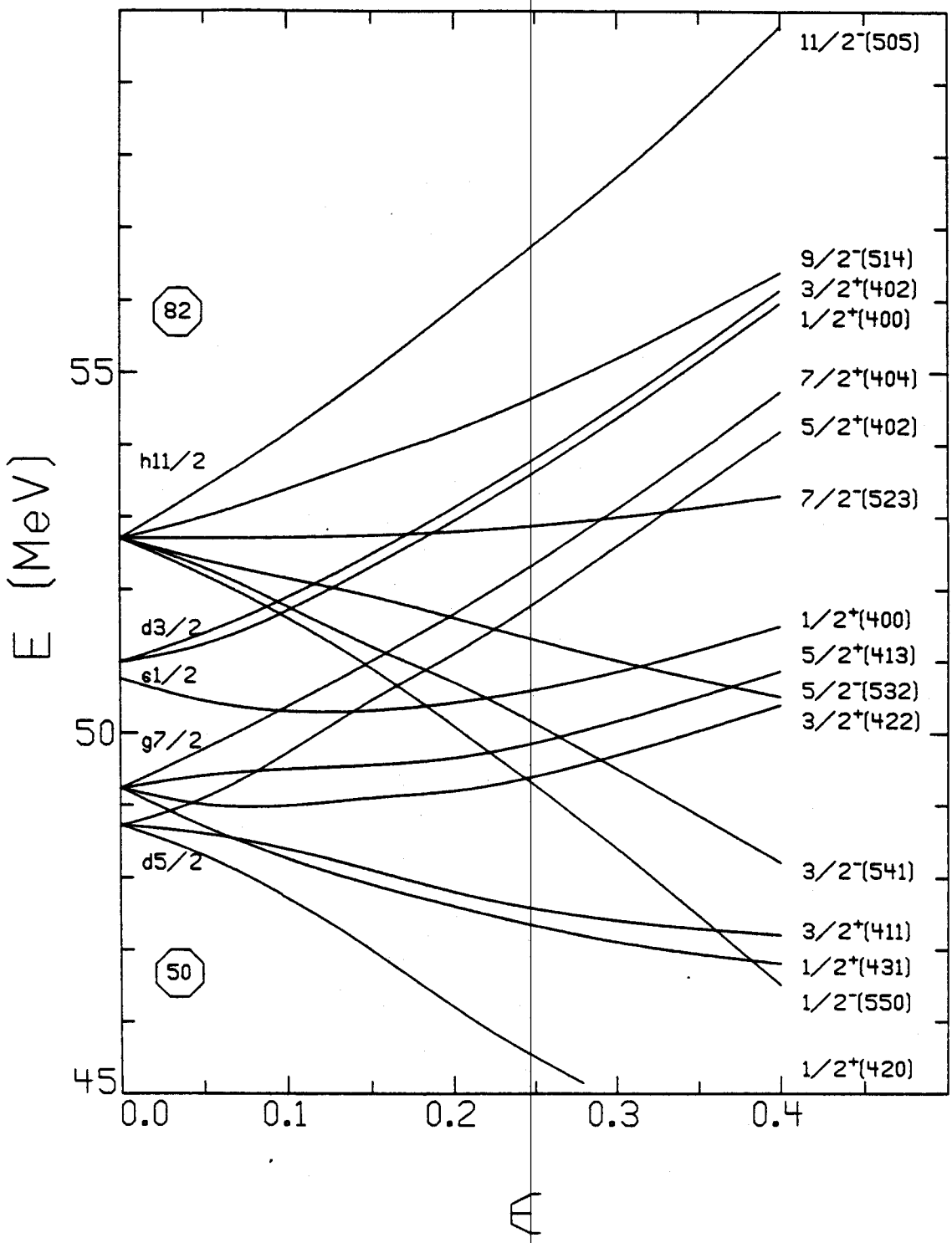

Figure VI-3 Nilsson diagram for odd neutrons

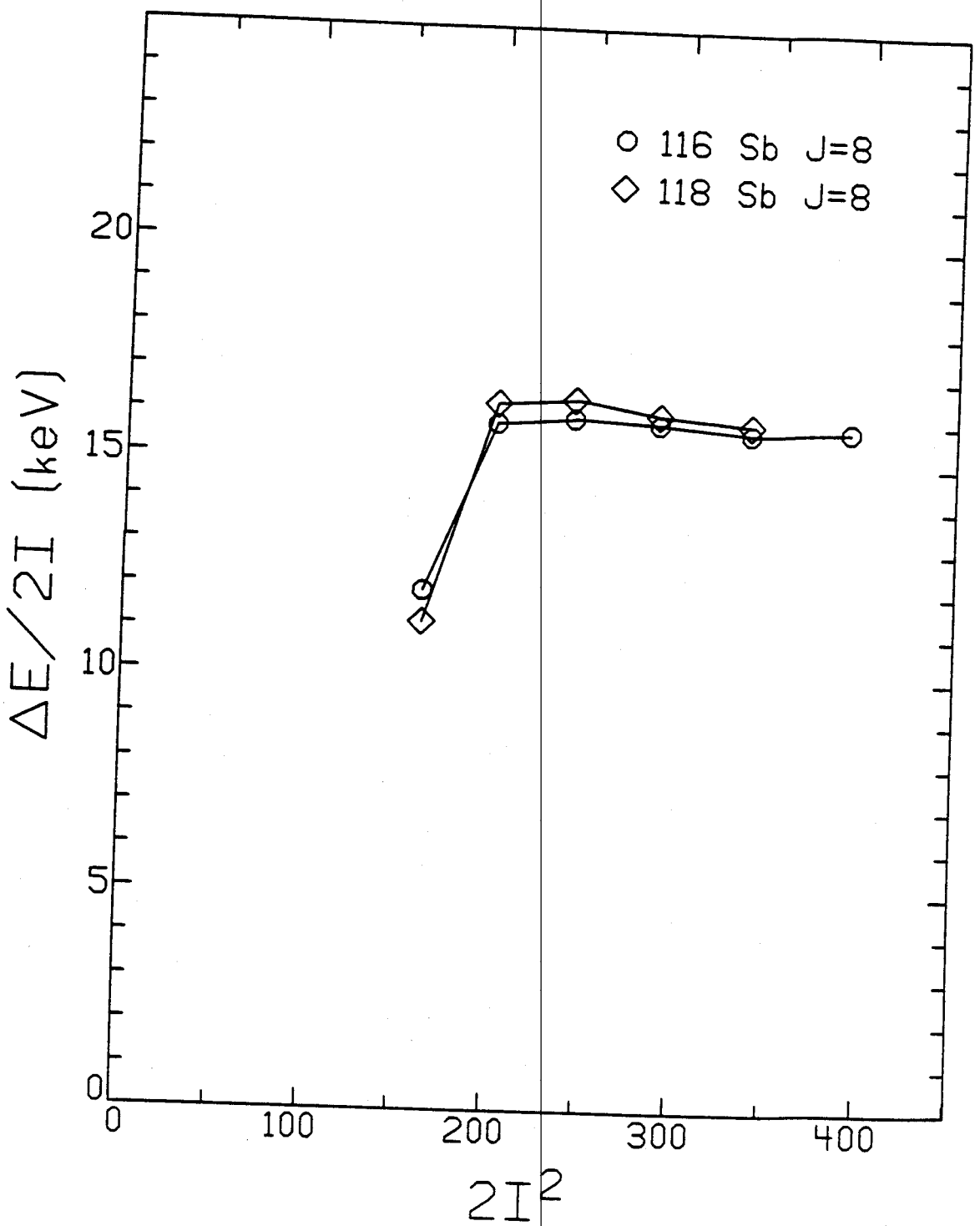

Figure VI-4 The rotational band spacing as a function of $2I^2$ for the J=8 bands in $^{116,118}Sb$

indicating that the strong coupling picture does indeed apply in this case. However, there are several reasons for arguing against this description.

The first consideration involves the moment of inertia. From the figure it can be seen that the rotational constant resulting from this K=8 band is about 16 keV. Comparing this moment of inertia result to an empirical relation determined from well deformed bands in the rare earth region,[36] the deformation is found to be extremely large ($\beta>0.5$). The likelihood of such a large deformation occurring so near the closed proton shell is rather remote.

The second reason involves the obvious anomaly in the first band member. Such anomalies are quite common in well deformed nuclei, and are explained by band mixing. In this particular case the existence of a K=9 band is required. The levels of such a band would mix with the levels of corresponding spin from the K=8 band. This would lower the energy of all levels except the K=8 bandhead for which there is no mixing. This produces a compression in the band's lowest transition. However, in this particular case using the strong coupling scheme, both the neutron and proton are already in the highest Ω components of their respective orbitals, and there is no way of producing a higher spin K=9 band.

The final argument against strong coupling involves a comparison with the bands in the neighboring odd mass nuclei. These odd mass bands although being strongly coupled do not

have energy spacings that follow the simple I(I+1) pattern of a single-particle coupled to an axially symmetric rotor. Calculations have been performed describing these bands using both the triaxial rotor model[7] and the axially symmetric model with band mixing.[12] In either of these cases it is unlikely that such perturbations of the simple rotor model would disappear upon adding an extra odd neutron. Consequently the non-trivial structure of the odd mass bands should lead to similar non-simple structure in the odd-odd bands. This argument indicates that the simple appearance of the odd-odd bands does not result from truly simple internal structure, but is only a chance occurance caused by several interfering effects. With this view there is good reason to consider alternatives to the strong coupling scheme.

The opposite extreme to a strongly coupled neutron is a rotationally aligned neutron. The data have features which tend to support such an interpretation. This can be seen in Figure VI-5, where the levels for the J=8 bands are plotted along with the levels of the $K^{\pi}=9^{+}/2$ bands from the odd mass Sb nuclei. The bands have all been normalized to the second level. The figure clearly shows the striking similarities in the energy spacing of the bands. This is what would be expected if the odd neutron was aligned. In this scheme the nucleus rotates in exactly the same manner as without the extra particle. The extra neutron is decoupled from the motion of the core and contributes a component to the total angular momentum, but has no effect on the rotational energies.

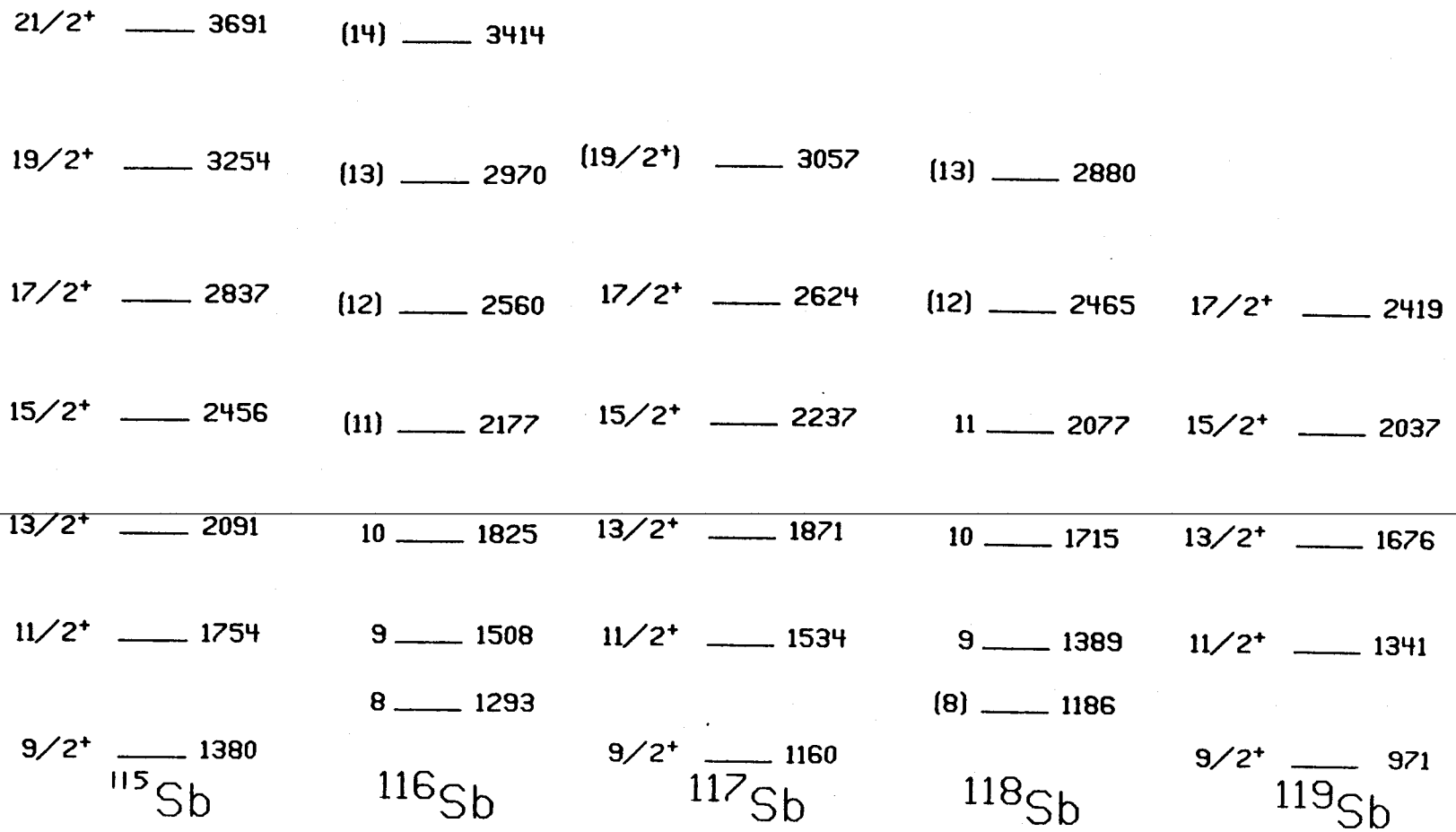

Figure VI-5 Levels for the J=8 bands in ^{116,118}Sb compared with levels for the $K^{\pi}=\frac{9}{2}^{+}$ bands in ^{115,117,119}Sb

With this interpretation it is clear that the proton is in the same $g_{9/2}$ hole state as occurs in the neighboring odd mass Sb bands. In addition the neutron must be in the unique-parity $1h_{11/2}$ orbital. This is consistant with the Fermi level being near the low-Ω components of this orbital. In this picture the proton is a strongly coupled hole state in the highest Ω component of the $g_{9/2}$ orbital, indicating deformation alignment. The $1h_{11/2}$ neutron is rotationally aligned, which implies that its spin is generally perpendicular to the direction of the proton's spin. The spin of the bandhead should then be approximately given by [21] $J \simeq (11/2)^2 + (9/2)^2 = 7.1$. This value is roughly consistent with the experimentally determined value of J=8.

This coupling scheme also allows a J=9 band, which can arise from a slightly different coupling of the neutron and proton spin. Although there is no experimental evidence to support the existance of such a band, it would be expected to lie somewhat higher in energy and would mix with the J=8 band. This could explain the experimentally observed compression of the lowest band transition.

The high moment of inertia is no longer a problem, since a large portion of the angular momentum for this band is coming from alignment of the neutron single particle angular momentum, rather than an actual increase in the rotational angular momentum. The observed moment of inertia represents only an apparent moment of inertia. The actual physical moment of inertia would be the same as determined

from the neighboring odd mass $K^{\pi}=9^{+}/2$ bands. Together these observations, although quite qualitative in nature, do give a consistent description of the J=8 bands.

Accepting this description for the J=8 bands, then eliminates one of the possible neutron configurations for the lower lying K=7 bands. The obvious differences in the energy spacing, as well as the absence of any interband connecting transitions, requires the K=7 and J=8 bands to have rather different intrinsic structure. This implies the K=7 bands do not involve the $1h_{11/2}$ neutron orbital.

The $5^{+}/2\{404\}$ Nilsson level is the remaining alternative for the neutron state, resulting in a band with both particles strongly coupled to give $K^{\pi}=7^{+}$. This assignment may explain the relatively long (21.7 and 12.6 nsec.) half-lives of the bandheads. Since the $5^{+}/2\{404\}$ Nilsson level at relatively small deformations is predominantly made up of the $2d_{5/2}$ shell model state and the high-spin states lying below this band are expected to involve the $1h_{11/2}$ neutron configuration, the decay of these bands would be hindered by l-forbiddeness.

This configuration assignment is also consistent with results obtained for the odd-neutron ^{117,119,121}Te nuclei.[37] These bands are observed built on $K^{\pi}=5^{+}/2$ and $7^{+}/2$ states. These are interpreted as rotational bands resulting from the $5^{+}/2\{402\}$ and $7^{+}/2\{404\}$ Nilsson levels. The former of these two is the same level as the proposed neutron configuration for the J=7 odd-odd bands. It is interesting to note that the $K^{\pi}=5^{+}/2$ band was excited to much higher spin and

with much greater intensity in ^{119}Te than in ^{117}Te. This is similar to the case in Sb where the proposed $K^{\pi}=7^{+}$ band in ^{118}Sb is populated more strongly than it is in ^{116}Sb. In addition the $K^{\pi}=7^{+}/2$ band was not excited in either ^{117,119}Te, but was in ^{121}Te. This is also consistent with the lack of observation of any $K^{\pi}=8^{+}$ strongly coupled bands in ^{116,118}Sb. Such a band however would be expected to appear in ^{120}Sb.

Figure IV-6 shows a plot of $\Delta E/2I$ as a function of $2I^2$ for the proposed $K^{\pi}=7^{+}$ bands in ^{116,118}Sb. Also included are the odd-neutron $K^{\pi}=5^{+}/2$ band in ^{119}Te and the odd-proton $K^{\pi}=9^{+}/2$ band in ^{115}Sb. (The band was chosen from ^{119}Te because in ^{117}Te it was only excited to the second band member. The ^{115}Sb band was chosen to represent the odd mass Sb bands because it has been excited to higher spin than in the others. However, it should be noted that this choice is unimportant since all of the odd-mass Sb bands are essentially identical.) From the figure it is clear that all of the bands have quite similar behavior. The moment of inertia increases sharply with spin at low spin values and then levels out at high spins. These similarities indicate that core deformation is approximately the same for all of these bands. This would be a surprising result if the closed shell Z=50 Sn nuclei were used for the Sb core. However, a more suitable core to describe the Sb bands is the even Te nuclei. This is because the proton configuration for the Sb bands is a hole state. So even though the spherical Sb states behave in a manner perscribed by particles coupled

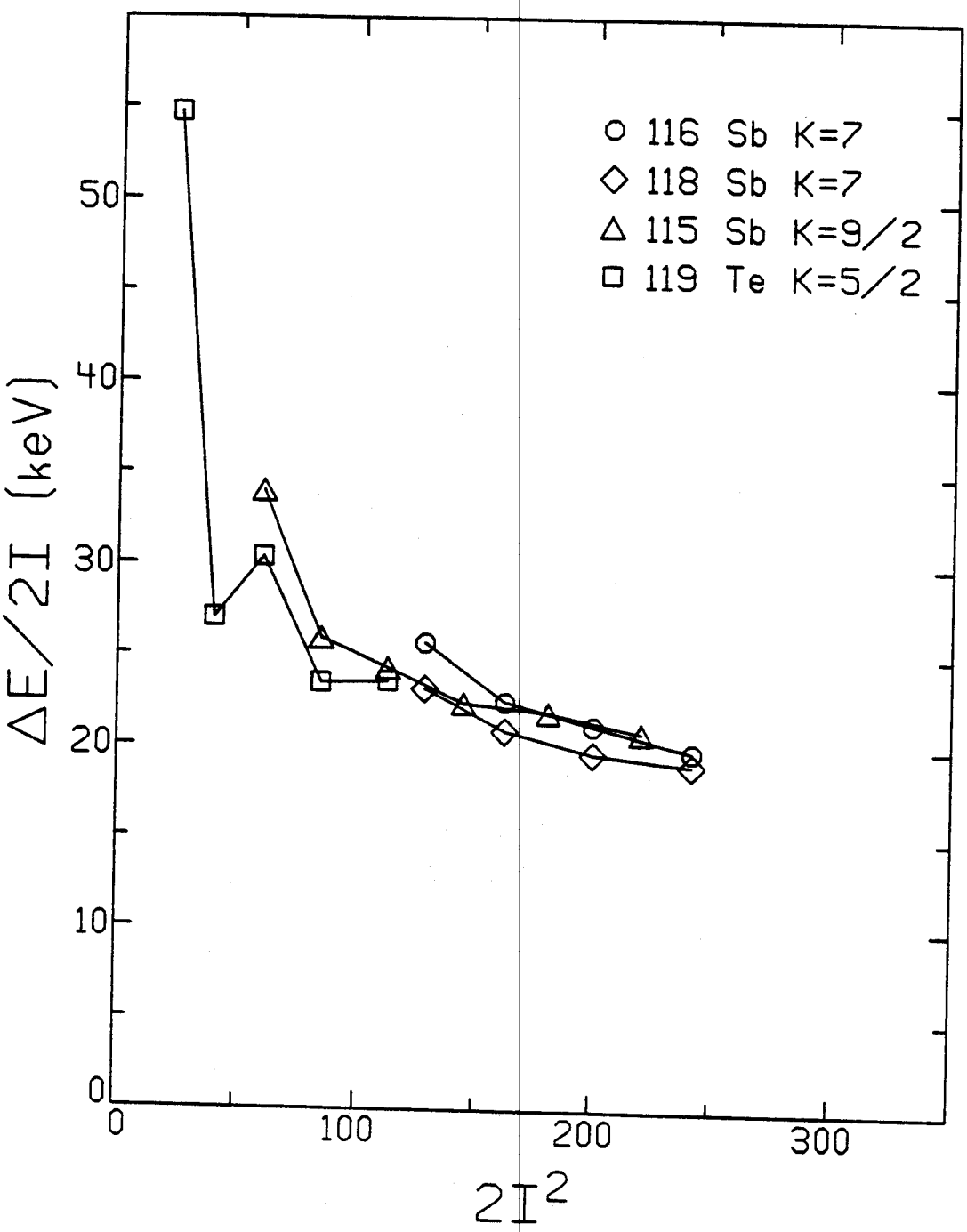

Figure VI-6

The rotational band spacing as a function of $2I^2$ for the K=7 bands in $^{116,118}Sb$ compared with the $K=\frac{9}{2}$ band in ^{115}Sb and the $K=\frac{5}{2}$ band in ^{119}Te

to a Sn core, the deformed states in these nuclei are better described as a hole state coupled to a Te core. Consequently assuming the proton-hole configuration, the similar behavior of the Sb and Te bands is expected to occur.

D. Summary

Experiments were performed studying the γ radiation following the proton, alpha, and lithium induced reactions which populated high-spin states in ^{116,118}Sb. Level energies, half-lives, spins, parities, and relative decay intensities were measured and qualitatively discussed in terms of the shell model and particle-plus-deformed-core model.

The level schemes display behavior than can be explained only by assuming the existance of both deformed and spherical states. Such coexistance of states has been observed in both the neighboring odd-proton Sb and odd-neutron Te nuclei. This study extends these findings to odd-odd Sb nuclei.

The spherical states can be adequately described in terms of either two-quasiparticle states, or two-quasiparticle states coupled to either collective or single particle excitations of the Sn core. The $1h_{11/2}$ neutron, unique-parity orbital is found to play a role in most of these states.

In addition to these spherical states two rotational bands are observed in each nuclei. These bands can be described in terms of a $g_{9/2}$ proton hole state strongly coupled to a deformed Te core. In the rotational model this state is described as the $9^+/2$ {404} Nilsson level. In

the case of the higher lying bands this proton state is coupled to a $1h_{11/2}$ rotationally aligned neutron state resulting in a $J^{\pi}=8^{-}$ band, that looks very much like the neighboring odd-mass Sb bands. This provides an example of the "conflicting case" in which one of the odd particles is aligned with the deformation while the other is aligned with the rotation.

The lower-lying bands exhibit somewhat different behavior and are best described as both particles being strongly coupled. In this case the proton and neutron are respectively in the $9^{+}/2\{404\}$ and $5^{+}/2\{402\}$ Nilsson levels, resulting in a $K^{\pi}=7^{+}$ band. This represents an example of the "peaceful case".

In conclusion, this picture provides a qualitatively good description of the odd-odd Sb nuclei, that is consistent with the behavior of the neighboring nuclei in this region.

REFERENCES

1. H. Toki, H. L. Yadav and A. Faessler, Phys. Letters 66B, 310 (1977).

2. A. K. Gaigalas, R. E. Shroy, G. Schatz and D. B. Fossan, Phys. Rev. Letters 35, 555 (1975).

3. C. B. Morgan, Thesis, Michigan State University, (1975).

4. K. Shafer, Thesis, Michigan State University, (1976).

5. W. B. Chaffee, Thesis, Michigan State University, (1975).

6. J. A. Carr, K. Shafer, R. A. Warner, Wm. C. McHarris and W. H. Kelly, MSUCL Annual Report, 87 (1974-76).

7. R. E. Shroy, A. K. Gaigalas, G. Schatz and D. B. Fossan, Phys. Rev. C19, 1324 (1979).

8. W. F. VanGunsteren, K. Allaart and E. Boeker, Nucl. Phys. A266, 365 (1976).

9. G. VandenBerghe and K. Heyde, Nucl. Phys. A163, 478 (1971).

10. W. D. Fromm, H. F. Brinkmann, F. Donau, C. Heiser, F. R. May, V. V. Pashkevich and H. Rotter, Nucl. Phys. A243, 9 (1975).

11. K. Heyde, M. Waroquier, H. Vincx and P. VanIsacker, Phys. Letters 64B, 135 (1976).

12. P. VanIsacker, M. Waroquier, H. Vincx and K. Heyde, Nucl. Phys. A292, 125 (1977).

13. J. Bron, W. H. A. Hesselink, H. Bedt, H. Verheul and G. VandenBerghe, Nucl. Phys. A279, 365 (1977).

14. M. G. Mayer, Phys. Rev. 74, 235 (1948).

15. O. J. Haxel, H. D. Jensen and H. E. Suess, Z. Physik 128, 295 (1950).

16. B. R. Mottelson and S. G. Nilsson, Mat. Fys. Skr. Dan. Vid. Selsk. 1, No. 8 (1959).

17. S. G. Nilsson, Mat. Fys. Medd. Dan. Vid. Selsk. 29, No. 16 (1955).

18. F. S. Stephens, Rev. of Mod. Phys. 47, 43 (1975).

19. J. Meyer-ter-Vehn, Nucl. Phys. A249, 111 (1975).

20. H. Toki and A. Faessler, Nucl. Phys. A253, 231 (1975).

21. H. Toki, H. L. Yadav and A. Faessler, Phys. Letters 71B 1 (1977).

22. P. M. Walker, S. R. Faber, W. H. Bentley, R. M. Ronningen, R. B. Firestone, and F. M. Bernthal, Phys. Letters 86B 9 (1979).

23. C. Flaum and D. Cline, Phys. Rev. C14, 1224 (1976).

24. CS8N computer program written by T. Sikkeland and D. Lebeck, LBL, University of California, Berkeley.

25. J. R. Grover, Phys. Rev. 157, 832 (1967).

26. J. R. Grover and J. Gilat, Phys. Rev. 157, 814 (1967).

27. T. Yamazaki, Nuclear Data Aβ, 1 (1967).

28. J. T. Routti and S. G. Prussin, Nucl. Instr. and Meth. 72, 125 (1969).

29. R. J. Gehrke and L. D. McIsaac, Aerojet Nuclear Co. Report 1088, 379 (1972).

30. C. Ekstrom, W. Hogervorst, S. Ingelman and G. Wannberg, Nucl. Phys. A226, 219 (1974).

31. R. Kamermans, H. W. Jongsma, T. J. Ketel, R. VanDerWey and H. Verheul, Nucl. Phys. A266, 346 (1976).

32. B. Skytte Jensen, O. B. Nielsen and O. Skilbreid, Nucl. Phys. 19, 654 (1960).

33. G. H. Carlson, W. L. Talbert, Jr., and S. Raman, Nucl. Data, 17 No. 1, 17 (1976).

34. P. T. Callaghan, M. Shott and N. J. Stone, Nucl. Phys. A221, 1 (1974).

35. Arie Van Poelgeest, Thesis, Vrije Universiteit te Amsterdam, (1978).

36. V. Hagemann, H. J. Keller, Ch. Protochristow and F. Stary, Nucl. Phys. A329, 157 (1979).